Unravelling of Sulphur Selenium unsaturation in $MoS_{(2-x)}Se_x$ with efficient acidic and alkaline Hydrogen Evolution Reaction (HER)

A thesis submitted towards partial fulfilment of the requirements for the degree of

Master of Technology in Nanoscience and Technology

Submitted by:

Tanbir Ahammed

Examination Roll No.: M4NST23021

Registration No.: 136442 of 2016-2017

Under the guidance of

Associate Prof. (Dr). Sourav Sarkar

School of Materials Science and Nanotechnology

Jadavpur University

Kolkata-700032

COURSE AFFLIATED TO

FACULTY OF INTERDISCIPLINARY STUDIES, LAW AND MANAGEMENT

JADAVPUR UNIVERSITY

KOLKATA-700032

INDIA

2023

MTech (Nanoscience and technology)

Course affiliated to

Faculties of Interdisciplinary Studies,

Law and Management

Jadavpur University

Kolkata, India

CERTIFICATE OF RECOMMENDATION

This is to certify that Tanbir Ahammed's thesis, **"Unravelling of Sulphur Selenium unsaturation in $MoS_{(2-x)}Se_x$ with efficient acidic and alkaline Hydrogen Evolution Reaction (HER)"** is genuine piece of work completed under our direction and supervision to full fill the requirement for the Master of Technology in Nanoscience and technology at the School of Materials Science and Nanotechnology for the academic year 2021-2023.

THESIS ADVISOR

Dr. Sourav Sarkar

School of Materials Science

and Nanotechnology

Jadavpur University, Kolkata-700032

DIRECTOR

Dr. Sourav Sarkar

School of Materials Science

and Nanotechnology

Jadavpur University, Kolkata-700032

DEAN

Faculties of Interdisciplinary Studies,

Law and Management

Jadavpur University, Kolkata-700032

M.Tech.(Nanoscience and Technology)
Course affiliated to
Faculty of Interdisciplinary studies,
Law and Management
Jadavpur University
Kolkata, India

CERTIFICATE OF APPROVAL **

This foregoing thesis is hereby approved as a credible study of an engineering subject carried out and presented in a manner satisfactorily to warranty its acceptance as a prerequisite to the degree for which it has been submitted. It is understood that by this approval the undersigned do not endorse or approve any statement made or opinion expressed or conclusion drawn therein but approve the thesis only for purpose for which it has been submitted.

Committee of final examination

for evaluation of Thesis

_____

_____

_____

_____

** Only in case the thesis is approved.

DECLERATION OF ORIGINALITY AND COMPLIANCE OF ACADEMIC ETHICS

I hereby certify that the undersigned candidate completed the literature review and original research for this thesis as a requirement for his **Master of Technology (Nano science and Technology)** studies during the academic year **2021–2023.**

All information in this document has been obtained and presented in accordance with academic standards and ethical conduct.

I further declare that I have properly cited and referred to all information and findings that are not original to this work, as required by these rules andconduct.

Name: TANBIR AHAMMED

Examination Roll Number: M4NST23021

Registration Number: 136442 of 2016-2017

Thesis Title: Unravelling of Sulphur Selenium unsaturation in $MoS_{2-x}Se_x$ with efficient acidic and alkaline Hydrogen Evolution Reaction (HER)

SIGNATURE: **DATE:**

Dedicated to my parents

ACKNOWLEDGEMENT

I express my gratitude to **Dr. Sourav Sarkar**, my academic advisor, for his unwavering support, enthusiasm, and extensive expertise over the course of my Master's studies and research. Throughout the process of working on my thesis, he provided steadfast support and guidance. I am appreciative for the insightful remarks you provided, as they served as a source of inspiration for my whole study endeavour. Furthermore, I would like to extend my appreciation to Professor Kalyan Kumar Chattopadhyay and the Thin Film and Nano Science Laboratory, as well as the Nanoscience and Nanotechnology Laboratory, for fostering a congenial working atmosphere for me.

I express my sincere appreciation to **Mr. Dipayan Roy**, who has served as my mentor, for his invaluable guidance and support in addressing various project-related challenges. Furthermore, I am grateful for his collaborative efforts, which have contributed significantly to the current state of the project.

I express my sincere gratitude to **Professor Kalayan Kumar Chattopadhaya, Dr. Sourav Sarkar, Dr. Mahua Ghosh, and Dr. Chandan Kumar Ghosh** for their invaluable help, unwavering support, insightful insights, and invaluable counsel. The learning atmosphere provided by the individuals was both supportive and conducive to growth, fostering a sense of enthusiasm inside me that motivated me to pursue the study issue with great passion.

I would like to express my sincere appreciation to Ratna Sarkar,Dimitra Das, Antika Das, Nabanita Sen, Suvankar Mondal, Bikram Kumar Das, Anibrata Banerjee, Suvankar Poddar, Suvra Pal, and Arnab Das, who are my seniors, for their invaluable contributions in making my project a really remarkable and unforgettable experience. I express my gratitude to Abhrajit Roy, Arnab Dhara, Aaishiki Saha, Sampurna Mukherjee and my fellow batchmates for their invaluable aid and unwavering support over the duration of this course. The completion of my project would not have been possible without their aid. Given the substantial assistance they have provided, my expressions of appreciation are inadequate.

In conclusion, I would want to sincerely acknowledge my parents and all those who have provided me with affection and assistance, expressing my deep appreciation for their unwavering love and support.

Abstract

The need for clean and renewable hydrogen energy and fuel cells is substantial due to their ample availability, significant energy density, and environmentally sustainable characteristics. In this abstract, a strategy has been presented for the synthesis of hierarchical $MoS_{(2-x)}Se_x$ by the manipulation of varying amounts of sulphur and selenium throughout the synthesis process. The reactive site for intermediate hydrogen (H*) adsorption in the overall hydrogen evolution process (HER) is confirmed by structural characterization and electrochemical experiments, which demonstrate the significance of S and Se unsaturation as well as their ratio. In the experimental study, it was observed that the introduction of a tiny amount of selenium (Se) into sulphur (S) resulted in a compound with the formula $MoS_{1.8}Se_{0.2}$. This compound exhibited improved catalytic activity for both acidic and alkaline hydrogen evolution reactions (HER), characterized by a low overpotential of -170 mV and -180 mV compared to the reversible hydrogen electrode (RHE) reference. At a current density of 10 mA/cm^2, the compound had a Tafel slope of 40 mV/decade for the acidic HER and 43 mV/decade for the alkaline HER. The facile hydrogen evolution reaction (HER) performances have been compared to those of pure MoS_2, $MoSe_2$, and $MoS_{(2-x)}Se_x$ materials with varying sulfur (S) and selenium (Se) ratios. Nevertheless, the enhanced electrode kinetics, increased density of catalytic active sites, and improved durability make $MoS_{1.8}Se_{0.2}$ a very competitive catalyst for the hydrogen evolution reaction, mainly due to its abundance in the Earth's crust.

Table of Content

Chapter2

Chapter 3

Chapter 4

Chapter 1
Introduction

1.1 Semiconductor:

A semiconductor is a substance characterised by its intermediate electrical conductivity, falling between that of a conductor and an insulator. A semiconductor refers to a substance, often a solid chemical element or compound, that has a band gap ranging from one to three electron volts (eV). The aforementioned components, namely transistors, diodes, and integrated circuits, include this particular element as a crucial constituent. Silicon is the predominant semiconductor material used in many applications, however other materials like germanium and gallium arsenide are also utilised. The manipulation of electrical conductivity in semiconductors may be achieved by the incorporation of dopants, which are impurities introduced into the material [1]. The aforementioned procedure is often referred to as doping, which facilitates the production of p-type and n-type semiconductors, serving as the fundamental components in several electrical devices. P-type semiconductors are characterised by an electron deficiency, while n-type semiconductors exhibit an electron surplus. The formation of a p-n junction occurs when p-type and n-type semiconductors are brought into contact. The aforementioned junction serves as a means of regulating the passage of electrical current and is the fundamental building block for several electronic apparatus, such as diodes and transistors. Transistors, which are constructed using semiconducting materials, are often regarded as one of the most crucial electronic devices [2]. Amplifiers or electronic switches are often used for the purpose of amplifying or altering electronic signals, and are ubiquitously present in almost all electronic apparatus. The first development of the transistor took place at Bell Labs in 1947, whereby a piece of germanium was used as the base material, and dopants were introduced to establish a p-n junction. The discovery of the transistor was a significant advancement in the field of electronics, subsequently catalysing the progress and proliferation of several additional semiconductor devices. Integrated circuits (ICs), which are essential components of contemporary electronics, are fabricated using semiconductors. An integrated circuit (IC) refers to a cohesive assembly of transistors, diodes, and other components that are interconnected to fulfil a designated purpose. The first integrated circuit (IC) was conceived and fabricated at Texas Instruments in the year 1958. This IC was constructed using a silicon substrate that was doped to create p-n junctions. Integrated circuits (ICs) have seen a significant reduction in size and an increase in complexity over the years, resulting in the ability to accommodate billions of transistors on a single chip.

The use of semiconductors has brought about a significant transformation in the realm of electronics, resulting in the creation of several products that have become indispensable in contemporary life, such as computers, cellphones, and TVs [3]. The semiconductor business is a significant worldwide sector, including prominent corporations such as Intel, Samsung, and TSMC. The semiconductor industry is anticipated to exhibit sustained growth due to the escalating demand for electronic

gadgets and the emergence of novel applications in the realm of renewable energy. Semiconductors find use in several domains, including but not limited to solar cells, LED lighting, and medical fields like X-ray imaging. The progress in semiconductor technology has resulted in the creation of smaller, more efficient devices that operate at higher speeds. This technological revolution has had a significant influence on both our everyday lives and many industries. The future prospects of semiconductors seem very promising due to their escalating utilisation in the domains of the Internet of Things (IoT) and artificial intelligence (AI).

Semiconductors play a crucial role in contemporary technology and are anticipated to maintain their significance in the foreseeable future. The capacity to regulate and modify the movement of electric current has facilitated the development of several electronic gadgets that have become indispensable components of our daily existence. The semiconductor industry plays a significant role in the global economy and is projected to sustain its growth in the coming years due to the emergence of novel semiconductor applications [4].

1.2 Nanoscience and Nanotechnology:

Nanoscience and technology include the examination and use of materials and systems at the nanometer level. A nanometer corresponds to a length that is equivalent to one billionth of a metre, approximately corresponding to the dimensions of an atom or a tiny molecule. The distinct characteristics shown by materials at the nanoscale are markedly unlike to those seen at the macroscale, hence contributing to the fast expansion and multidisciplinary nature of nanoscience and technology.

Nanoscience and technology exhibit considerable promise across several domains, including medical, electronics, energy, and materials science. In the field of medicine, researchers are now exploring the use of nanoparticles as a targeted medication delivery system for particular cellular targets inside the human body. The field of electronics is now seeing advancements in the development of semiconductor nanowires, which are being explored as a potential component for computer chips. These nanowires are used to create minuscule transistors. Nanomaterials, particularly carbon nanotubes, are now being investigated in the field of energy as potential enhancements for solar cells and batteries. Nanocomposites with enhanced strength and durability are now under development in the field of materials science [5].

Nanoscience and technology are also contributing to the development of novel materials that possess distinctive characteristics, including catalysts, drug delivery systems, imaging and diagnostic instruments, among other applications.

The realm of medicine has significant potential for the use of nanoscience and technology. Nanoparticles has the capacity to be purposefully designed for the targeted delivery of pharmaceutical agents to cancerous cells, therefore mitigating adverse effects and enhancing therapy efficacy. Furthermore, the use of nanoparticles presents the opportunity to develop diagnostic instruments capable of early illness detection. The discipline of electronics stands to be revolutionised by nanoscience and technology. Nanomaterials, exemplified by carbon nanotubes and graphene, possess distinctive electrical characteristics that have the potential to enhance the performance of computer processors in terms of speed and efficiency. Furthermore, the use of nanoscale transistors has the potential to facilitate the advancement of electronic gadgets with significantly reduced power consumption [7-9].

Although nanoscience and technology provide promising advantages, there are also apprehensions about their possible hazards. Several research have posited that the exposure to nanoparticles may give rise to adverse health effects, whilst other investigations have expressed concern over the possible ecological ramifications of nanomaterials. Hence, it is essential to persist in doing more study on the possible hazards and advantages of nanoscience and technology to facilitate the development of secure and efficient applications [5].

In general, the subject of Nanoscience and technology is seeing significant growth and has the capacity to bring about transformative advancements across several sectors, including medical, electronics, and materials science. Currently, scholars are actively investigating novel applications of nanomaterials in order to develop innovative goods and enhance the performance of existing ones. Although there exist some apprehensions about the possible hazards associated with nanoscience and technology, it is important to persist in the examination of this discipline to comprehensively comprehend its prospective advantages and disadvantages [8].

1.3 Why Nanotechnology?

Precise and controlled fabrication or assembly of atoms and molecules at nanometre (10^{-9} m) dimension into novel materials and devices with unique properties. Nanotechnology involves the understanding, manipulation, and utilization of matter at the nanoscale, where the properties of materials differ from their bulk counterparts. By engineering and controlling nanoscale structures and devices, scientists can develop innovative solutions across various fields, including electronics, materials science, medicine, energy, and environmental science. It offers unprecedented control over matter's fundamental building blocks, enabling the creation of novel materials, sensors, devices, and systems with enhanced functionalities and performance [10].

The electron transfer properties of macro sized and nano sized particles of the same materials are different.

MATERIALS	MACRO-SIZE	NANO-SIZE
Led sulphide	Is an insulator	Becomes conductor
Iron oxide	Band gap is 1.95 eV	Band gap is 3.1eV
Carbon	Electron emission at 2500 V	Electron emission at much lower voltage 2.5 V

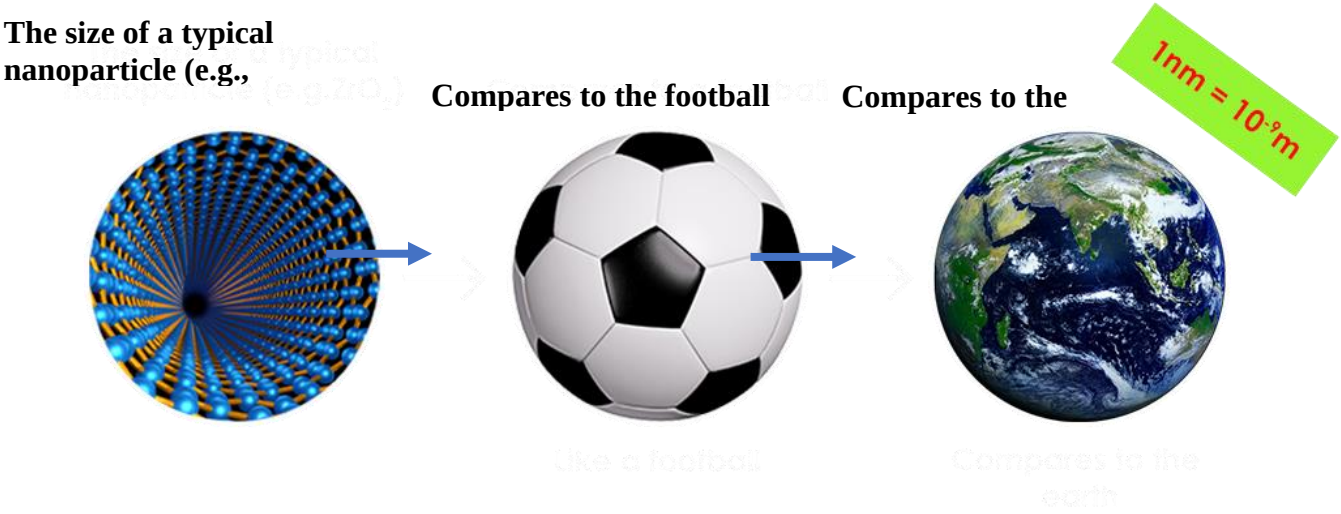

1.4 The Evolution of Nanotechnology and Its History:

Research on the nanometer scale is not a new topic of study, even if nanotechnology is. The study of biological systems and the creation of several materials, such as colloidal dispersions, metallic quantum dots, and catalysts, have long made use of the nanometre regime. Data from the past shows that nanotechnology has been around since the beginning of human society. The early manipulation of materials and empirical knowledge of artisans served as the foundation for early instances of nanostructured materials [11]. The most important scientific discoveries with clear applications and implications in nanotechnology emerge in the modern era as a result of inventions and tremendous development of spectroscopic and characterization tools, such as Transmission Electron Microscopy, Field Emission Scanning Electron Microscopy, and so forth.

4th century: Glass coloured by Ag and Au nanoparticles (Lycurgus cup, British Museum).

9th to 17th century: Glowing, glittering "lustre" glazes.

About 2000 years ago: In ancient Egypt, common men use nanoparticles called galenite (lead sulphide), a dying paste to their hair black, a few nanometres in size. They were able to make this by reacting lime, lead oxide and small amount of water. More than 1000 years ago: Chinese are known to use Au nanoparticles as an inorganic dye to introduce red colour into their ceramic porcelains.

19th century: Photography using Ag nanoparticles.

1857: Colloidal dispersion of gold (Au) prepared by Michael Faraday.

1931: The first Transmission Electron Microscope was built by Max Knoll and Ernst Ruska in 1931, with this group developing the first TEM with resolution greater than that of light in 1933 and the first commercial TEM in 1939. In 1986, Ruska was awarded the Nobel Prize in physics for the development of Transmission Electron Microscopy.

1936: Erwin Muller invented the field emission Microscope.

1950: Victor La Mer and Robert Dinegar developed the theory and a process for growing monodisperse Colloids.

1956: Arthur von Hippel introduced "molecular engineering ".

1958: Jack Kilby built the first integrated circuit.

1959: Richard Feynman projected engineering at the atomic scale.

1965: Moore's Law.

1972: Field Emission Scanning Electron Microscope was invented by Albert with the help of Hitachi

1974: Professor Norio Taniguchi at the University of Tokyo first invented the term "nanotechnology".

1981: Gerd Binning and Heinrich Rohrer invented the Scanning Tunnelling Microscope. They awarded Nobel Prize in physics in 1986.

1985: Discovery of Buckminsterfullerene (C60) at Rice University by Richard Smalley, Robert Curl, James Heath, Sean O'Brien, and Harold Kroto.

1986: Gerd Binning, Calvin Quate, and Christoph Gerber invented the atomic force Microscope.

1991: Carbon nanotube was discovered by Prof. Sumio Iijima.

1992: C.T. Kresge and colleagues discovered the nanostructured MCM-41 and MCM-48.

1993: Invention of controlled synthesis of nanocrystals.

1998: Dr. Nadrian, C. Seeman and his co-workers at New York University announced in January a major advance along one potential path toward molecular nanotechnology that involves making devices from branched DNA molecules.

1999: Dip pin nano lithography was invented by the Mirkin Group.

2003: 21st century Nanotechnology Research Report.

2005: DNA based computer and "algorithmic self-assembly".

2007: Lithium-ion battery with a common type of virus.

2009: Several DNA-like robotic Nanoscale assembly devices.

2010: Graphene, two dimensional, one of the allotropes of carbon was discovered in 2004 by Ande Geim and Konstantin Novoselov at the University of Manchester and they were awarded Nobel Prize in physics in 2010.

2014: The NNI release the updated 2014 Strategic plan.

1.5 Grouping of nanomaterials

The fields of nanoscience and nanotechnology have expanded quickly over the last several decades as a result of the identification of novel synthesis routes, characterisation methods, and manipulation tools. Thin films, nanowires, and nanoparticles are only a few of the many types of nanoscale structures. When referring to nanoparticles, which are effectively zero-dimensional systems, the phrase "quantum dot" is widely used [12]. The novel characteristics of the aforementioned systems, which are only applications of Basic Physics, have a thorough explanation thanks to theoretical research. Understanding these systems requires a short explanation of the density of states (DOS) of quantum dots (0 dimension), quantum wires (1 dimension), and quantum wells (2 dimensions).

The number of states per interval of energy at each energy level that are accessible to be occupied is referred to as the density of states (DOS) of a system in solid-state and condensed matter physics.

The DOS is determined by the thing's own dimensional bounds [13].

Dimensions are shown using the units of DOS (Energy-1 Volume-1). In the limit when the system has two dimensions, a volume becomes an area, and in the limit where the system has one dimension, a length. It is important to keep in mind that the volume under consideration is the volume of k space, or the region enclosed by the system's constant energy surface, and that this volume is determined through a dispersion relation between E and k. The dispersion relation for electrons inside a material is governed by the electronic band structure [14].

The available electron states in a system can be calculated by the well known Schrodinger's equation:

$$HT = ET.$$

The general expression to obtain the density of states in k-space/volume is as follows:

$$N(E)dE \propto E^{(d/2 -1)}\, dE \qquad d=1,2,3$$

In this situation, where d is the degree of dimension, the energy is computed from the top of the valence band for holes and the bottom of the conduction band for electrons. In the three-dimensional (3-D) system, N(E) is an energy function with a smooth square-root form. A 2-D system varies greatly from a 3-D system because N(E) in a 2-D system is constant. The energy spectrum is quasi-continuous even though the density of states in a 2-D system is a step function [15]. Every time we go to a system with smaller dimensions, the DOS's reliance on energy changes by an order of magnitude, or E-1/2.

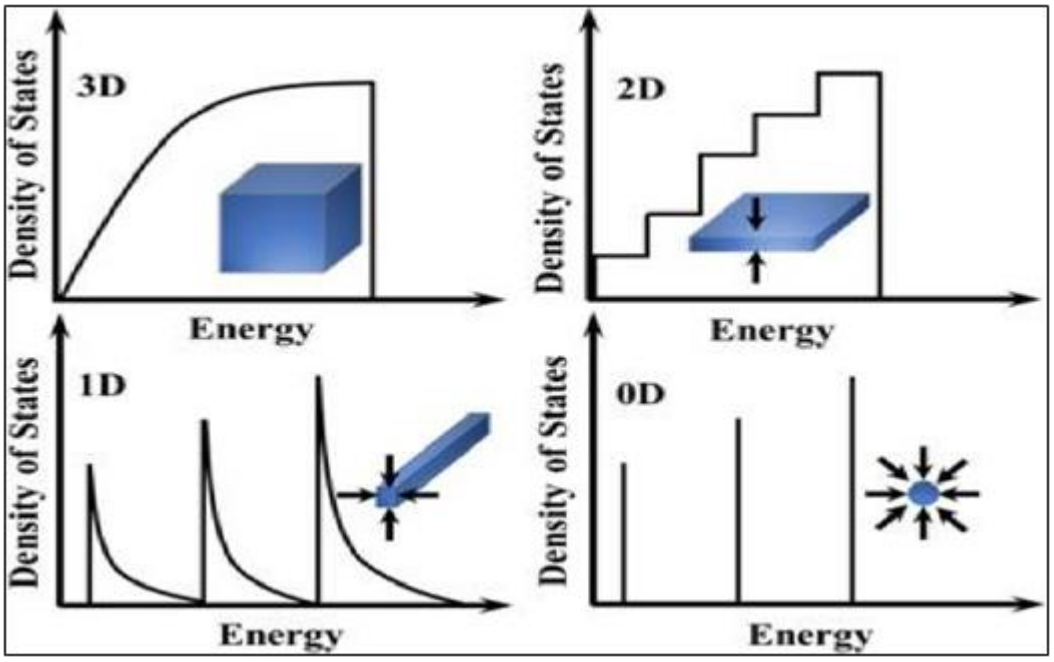

Fig 1.1 Schematic illustration of structural dimensionality of materials with density of states[16]

Now it's time for a brief examination of the "quantum size effect". Materials' electrical properties are changed while their particle sizes are significantly decreased to accomplish this. This impact is irrelevant if the decrease in dimension is limited to the macro to micro range. However, at the nanoscale, the quantum impact is clearly visible. When the diameters of the nanoparticles are comparable to the Bohr excitonic radius (rB) of such materials, the quantum confinement effect modifies the electrical structure of nanocrystals.

If the particle radius (r) in the nanocrystalline materials is less than the Bohr radius (rB), strong quantum confinement phenomena take place. It has been discovered that particles with radii higher than the Bohr radius (r>rB) exhibit mild quantum confinement effects.

Many physical properties, including electrical, optical, and mechanical ones, change at the nanoscale level as compared to a macroscopic system. For instance, a rise in the surface to volume ratio affects the materials' thermal, mechanical, and catalytic characteristics. Both the properties of charge transport in nanodevices and the rate of reaction diffusion for nanostructured materials accelerate.

1.5.1 Zero dimensional materials (0-D)

Any material greater than 100 nm in which all dimensions are measured at the nanoscale is referred to as 0-D. The most prevalent kind of zero-dimensional nanomaterials are nanoparticles. Nanoparticles may be constructed of metallic, ceramic, or polymeric materials and come in a wide range of forms and sizes. They can also exist alone or as a component of a matrix. They may be composed of one or more chemical components and can also be amorphous, crystalline, single-crystalline, or polycrystalline. In 0-D nanomaterials, when all dimensions are nanoscale, an electron is limited in three-dimensional space. The electrons don't migrate or get delocalized [17].

1.5.2 One dimensional materials (1-D)

As a consequence, nanoparticles are created that have a shape similar to a needle in one dimension that is not tiny. One-dimensional materials include nanotubes, nanorods, and nanowires. 1-D nanomaterials may be freestanding substances or embedded in other media, and they can be metallic, ceramic, polymeric, single-crystalline or polycrystalline, chemically pure or impure [18], amorphous or crystalline, single-crystalline or polycrystalline, or any combination of these. In 1-D nanomaterials, delocalization occurs along the nanomaterial's long axis of the nanowire, nanorod, or tube, while electron confinement occurs in 2-D.

1.5.3 Two dimensional materials (2-D)

Materials that do not possess dimensional restrictions within the nanoscale range are often referred to as bulk nanomaterials. These materials may be characterised by their three dimensions, which are arbitrarily chosen to be more than 100 nm. Materials may possess a structure that is nanocrystalline or exhibit properties at the nanoscale. Bulk nanomaterials consist of nano-sized crystals arranged in different orientations, often exhibiting nanocrystalline formations [19]. In relation to the existence of nanoscale attributes, 3-D nanomaterials include various structures such as multinanolayers, clusters of nanowires and nanotubes, as well as distributions of nanoparticles. The electrons in 3-D nanomaterials exhibit complete delocalization.

1.6 Optical and Electrical properties of nanomaterials

1.6.1 Transmittance and Absorption

The transmission and absorption characteristics of every substance are affected by the size of its particles. Nanoscale materials exhibit distinct properties. The manipulation of external factors will have an impact on these characteristics. The confinement of carriers at the quantum level may occur due to variations in particle size, and this phenomenon tends to intensify as the dimensions decrease [20]. The presence of dopant inclusions has the potential to modulate the band gaps. The difference in band gap is often attributed to the alteration of lattice properties via processes such as annealing [21,22] or impurity doping [23,24].

1.6.2 Electrical conductivity

The charge transfer phenomena in nanoscale materials is primarily influenced by the presence of grain boundaries [25]. The interface of the grain boundary has a notable influence because to its elevated density of defects, such as vacancies, dangling bonds, and vacancy clusters [26]. Consequently, when an external field is present, the transportation of charge at interfaces across grain boundaries may occur by mechanisms such as dipole reorientation, electronic relaxation polarisation, and space charge dispersion. The presence of grain boundary defects has a notable impact on the alteration of a material's dielectric characteristics under external heating conditions.

1.7 What are the reasons for studying and using 2-dimensional materials?

The field of nanomaterials, a branch of material science, centres on the investigation of substances that possess at least one dimension inside the nanoscale scale [27]. At this particular magnitude, the quantity

of atoms or molecules comprising the substance is associated with discernible changes in its physicochemical characteristics and reactivity. Examples of size-effect properties may be seen in the quantum confinement of semiconductor particles, the surface plasmon resonance of metal nanoparticles, and the superparamagnetism of magnetic nanomaterials.

When just one dimension is restricted, the material exhibits a layered or two-dimensional (2D) structure. When both dimensions are restricted, the material assumes a wired or one-dimensional (1D) configuration. Finally, if both dimensions are confined to a few nanometers or less, the material is sometimes denoted as zero-dimensional (0D).

Hence, a crucial determinant in characterising the properties of a material is its dimensionality, rather than only its size. This statement has particular significance in the context of sp2 carbon materials (see Figure 1.2), since they exhibit a wide range of distinct properties, including 0-dimensional (0D) fullerenes, 1-dimensional (1D) nanotubes, 2-dimensional (2D) graphene, and 3-dimensional (3D) graphite. Moreover, the instance of carbon provides a compelling illustration when considering the sequential progression of discoveries pertaining to the diverse dimensional configurations of a certain substance. Graphite has been widely used in industrial applications since the sixteenth century, serving as a crucial component in the production of steel, as well as finding utility in brake linings and functioning as a dry lubricant in diverse equipment. However, the discovery of fullerenes in 1985 significantly expanded the existing knowledge of carbon allotropes, leading to the consideration of the potential existence of carbon nanotubes, which were first detected in 1991.

The use of individual graphite layers as initial substances for theoretical examinations of graphite, fullerenes, and nanotubes has been documented. However, the successful isolation of a single-layer graphene sheet was not achieved until 2004 [28]. The current surge of scholarly publications on graphene reflects both the intrinsic scientific curiosity around this substance and its prospective implications in several technological domains. It is expected that two-dimensional materials will have a substantial impact on several fields, such as electronics, gas storage or separation, catalysis, high-performance sensors, support membranes, and inert coatings, among others.

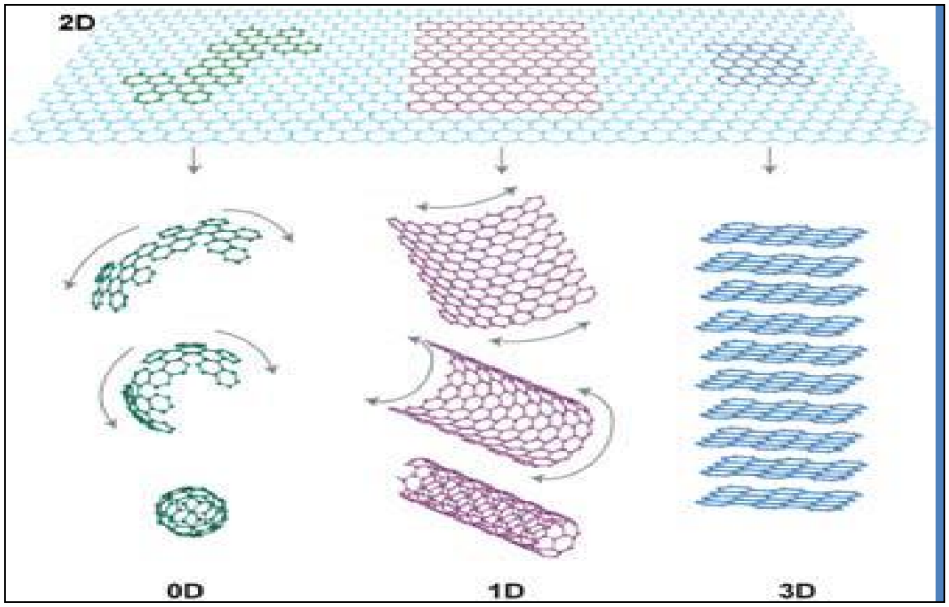

Fig 1.2 Graphene can be envisaged as a 2D material for carbon materials among all other dimensionalities. It can be wrapped up into 0D bucky-balls, rolled into 1D nanotube or stacked into 3D graphite [29].

Numerous publications and studies have extensively discussed the fabrication methods and physical properties of graphene. The discovery of these results has stimulated the creation of other innovative two-dimensional materials. However, the existing body of literature on this topic remains limited and fragmented. This review aims to emphasize the existing body of literature on ideas and techniques pertaining to the isolation and characterization of graphene. It proposes the application of these established approaches to a novel group of 2D materials, with the objective of achieving a comprehensive perspective on the subject matter. Furthermore, novel perspectives and potential applications for these two-dimensional materials are presented.

The alteration of some material properties is seen when size constraints are imposed on one or more dimensions. Hence, it is usually observed that two-dimensional (2D) materials exhibit distinct characteristics when compared to their bulk counterparts. The different optical and electrical characteristics of a material may be attributed to the confinement of electrons and the lack of interlayer interactions. Interlayer interactions, while normally modest, play a key role in shaping the band structure. The changes in properties, such as mechanical and chemical reactivity, are primarily induced by geometric factors and the significant surface-to-volume ratio, which may approach infinity in very thin materials.

1.8 Introduction of $MoSe_2$:

The first acquisition of a graphene monolayer occurred in 2004, as shown by Novoselov and Geim et al. [1]. This discovery provided evidence for the stable existence of two-dimensional (2D) crystals in the

natural world. Graphene has a plethora of distinct physical and chemical features that are not seen in other carbon-based materials. For instance, the presence of a flawless crystal structure imparts favourable electrical conductivity [2–4]. Additionally, the formation of a stable hexagonal plane structure through internal carbon atoms grants it remarkably high compression and tensile strength [3,5]. Moreover, the inherent stability of its lattice structure contributes to its exceptional thermal conductivity [3,6]. Furthermore, graphene exhibits notable performance in terms of light transmittance, ferromagnetism, and gas barrier properties [30]. Graphene has garnered significant attention among the scientific community because to its distinctive structure and exceptional features. Simultaneously, researchers have shown significant interest in the 2D transition metal dichalcogenides (2D-TMDCs), which possess graphene-like structures.

There exists a diverse range of over 40 varieties of transition metal dichalcogenides (TMDCs) [33]. These TMDCs are characterized by a fundamental chemical formula of MX_2, where M represents a transition metal element such as Mo, W, Nb, Re, Ni, or V, and X represents a sulphide element such as S, Se, or Te. The sandwich structure of single-layer transition metal dichalcogenides (TMDCs) is composed of two layers of X atoms enclosed by a layer of M atoms, denoted as "X-M-X". The use of this technology is prevalent across several disciplines, including photocatalysis, energy storage, solid state lubrication, microelectronics, and optoelectronics [32,13]. In recent years, MoSe2 has emerged as a prominent study subject within the class of transition metal dichalcogenides (TMDCs) due to its exceptional physical and chemical characteristics, as well as its remarkable potential for many applications across numerous domains. MoSe2 is a grey powder with a density of 6.0 g/mL at ambient temperature (25 °C) and a melting point of 1200 °C (0 °C). It is classified as a compound that belongs to the hexagonal crystal structure. The mixture of Mo and Se, with a molar ratio of 1:2, mostly produces MoSe2 when subjected to temperatures ranging from 800 °C to 1150 °C. The MoSe2 block exhibits a characteristic sandwich structure, whereby the layers are held together by relatively weak van der Waals forces. Consequently, it was first used as a solid lubricant. The advancement in the field of chemical stability has paved the way for exploring its use in the development of lubricants capable of withstanding high temperatures and pressures [33,34]. When the number of layers of MoSe2 is decreased from several layers to a small number of layers or even a single layer, there is a change in the electron band gap from the initial indirect band gap of 1.1 eV to a direct band gap of 1.55 eV (references 35-40). The use of single-layer MoSe2, a novel semiconductor material, has gained attention due to its notable photoelectric conversion efficiency. Consequently, it has been employed in the fabrication of electronic devices with enhanced efficiency. The interlayer spacing of MoSe2 is observed to be 0.646 nm, which is notably larger compared to the interlayer spacing of graphite (0.335 nm) and MoS2 (0.615 nm) [41,42].

The 2D MoSe2 material exhibits several properties, including surface and interface effects, small size effects, quantum size effects, and macro quantum tunnel effects. In comparison to graphene, $MoSe_2$ exhibits a somewhat broader prohibited bandwidth, which assumes a more significant role in the operation of field effect transistors and low-power electron devices. In addition to its unique features, $MoSe_2$ exhibits characteristics such as the back gate effect and solid lubrication, which are not seen in other transition metal disulfides. The synthesis methodology used for $MoSe_2$ has similarities to those of other two-dimensional (2D) materials. The techniques often used in this field include mechanical stripping, ion insertion, vapour deposition, hydrothermal, and molecular beam epitaxy, among others. Every approach has its own limitations and drawbacks. Currently, the primary challenge is in devising methods to produce large-area films or samples with few agglomerations, while maintaining cost-effectiveness and high efficiency. Simultaneously preparing several samples poses some challenges. Fortunately, the research conducted by McCreary K. M. et al. [42] and Sun L. et al. [44] has provided valuable insights that might potentially assist in addressing these challenges.

1.8.1 Different synthesis methods of $MoSe_2$:

*The synthesis process included the use of both top-down methods, including mechanical exfoliation [44, 45] and chemical exfoliation [46– 48], as well as bottom-up approaches, such as chemical vapour deposition on substrates [49, 40] and chemical synthesis [50,42]. Various approaches have been used for the synthesis of MoS2 as a co-catalyst.

- ***Mechanical stripping:*** The first use of the mechanical stripping technique was seen in the manufacture of graphene. Subsequently, due to its uncomplicated operation and the attainment of a uniform film surface, the use of this technique was swiftly extended to several additional two-dimensional (2D) materials. The process of synthesising MoSe2 using the mechanical stripping approach involves first growing a block on a suitable substrate. Subsequently, the block is repeatedly affixed to a thin laminar slice using specialised tape. Finally, the top laminar slice of the tape is transferred onto the desired substrate. In this study, Philipp Tonndorf et al. used a mechanical stripping technique to fabricate monolayer and few-layer flakes of MoSe2. Strong photoluminescence emission was obtained from monolayer MoSe2, suggesting that it had the characteristics of a direct gap semiconductor [51]. The mechanical stripping approach has many drawbacks, notably including poor production efficiency and the inability to achieve industrialized mass production synthesis [52].
- ***Intercalation stripping****:* The intercalation stripping method involves the insertion of cations with a small radius between the layers of MoSe2 in order to increase the interlayer distance. This process weakens the van der Waals force between the layers, allowing for their separation through

ultrasonic vibration. Consequently, this method enables the production of a reduced number of layers, or even a single layer, of MoSe2. Zeng et al. (37) devised a regulated technique for the injection of Li^+. The exact control of Li^+ may be achieved during the insertion and discharge of 2D materials by using them as cathodes in electrochemical devices.

- ***Chemical vapor deposition (CVD):*** Chemical vapour deposition (CVD) is a technique used for the deposition of films onto substrate surfaces. This process typically involves the reaction of a gas combination, which includes a reducing gas and an oxide-containing film element. Using the synthesis of MoSe2 thin film as a case study, the procedure involves placing MoO_3 on the central region with a high temperature, while the Se powder is positioned on the left most part with a lower temperature. Additionally, a mixture of H_2 and Ar gases is used as the transport medium.
- ***Hydrothermal:*** The hydrothermal technique is a chemical process conducted inside a sealed pressure vessel, using high temperature and high-pressure conditions, with water serving as the solvent. The synthesised crystal exhibits a crystal face characterised by reduced thermal stress and a decreased presence of internal flaws. The process of changing the solvent to a non-aqueous solvent is referred to as solvent heating. In their study, Xiu-Li Luo et al. (40) used a two-step hydrothermal technique to synthesise the peanut-like MoSe2/BiVO4 photocatalyst. The MoSe2/BiVO4 combination exhibited significantly enhanced photocatalytic activity in the breakdown of glyphosate under visible light compared to both bare BiVO4 and MoSe2. The photocatalyst that exhibited the best efficiency among all the produced samples was 0.15MoSe2/BiVO4. The hydrothermal approach was used by Iram Siddiqui et al. [54] to successfully synthesise broom-shaped MoSe2 nanostructures with an average diameter and length of around 150 nm and 10 μm, respectively. The experimental results demonstrated a high level of performance in the degradation of organic dyes. Using methylene blue as an illustrative example, it was observed that during the first 20-minute period, the efficacy of methylene blue was determined to be 89.91%.
- ***Molecular beam epitaxy:*** The study conducted by Akihiro Ohtake et al. [55] used molecular-beam epitaxy as a method for fabricating MoSe2 films. This approach facilitated the production of highly orientated film samples. The usage of Si(111) surface, ended by a GaSe bilayer, effectively suppressed the chemical interaction between Mo and Si. In a study conducted by Zhang et al. (56), it was reported that they successfully fabricated MoSe2 films of exceptional quality using a layer-by-layer growth process. Simultaneously, the direct observation of the change from an indirect band gap to a direct band gap occurred for the first time. Numerous researchers have documented alternative approaches for the synthesis of MoSe2. Fabian Gohler € er al [57] revealed a novel way to prepare MoSe2 films. The researchers opted for epitaxial graphene on SiC(0001) as the substrate and used modified elemental reactants (MER) precursors for the growth of the films. The target MoSe2 film was recognised as the grown film via the use of XPS and Raman spectroscopy. XPS analysis revealed an average film thickness of around one monolayer. Bougouma et al. (58)

conducted the synthesis of monocrystalline and polycrystalline MoSe2 powders using the chemical vapour transmission method. In a study conducted by Hankare et al. (59), molybdenum selenide was synthesised under low-temperature conditions in an alkaline environment, resulting in the material exhibiting N-type transmission characteristics. In the scholarly literature of S. N. In a study conducted by Wang et al. (60,61), the deposition of molybdenum selenide flakes onto glass or stainless steel substrates was achieved using a suppressed precipitation technique. The resulting films exhibited a consistent distribution of grains throughout. Feng Q et al. [48] achieved the synthesis of MoS2(1-x)Se2x monolayer alloys with varying edge orientations by manipulating the deposition temperature in physical vapour deposition. The photoluminescence of the band-gap may be adjusted in a continuous manner within the range of 1.86 to 1.55 electron volts (eV). The research conducted by the authors offers a viable approach to synthesising $MoSe_2$ with varying edge orientations.

1.9 Objective of the work

- The primary aims of this thesis are as follows:

1. To synthesize MoSSe nanomaterials.
2. S-Se unsaturation by simple Hydrothermal route and study its electrochemical property.

- The specific objective of this work is as follows:

1. To study various structural, morphological and surface analysis of the prepared samples.
2. To study HER kinetics of different MoSSe sample.

One of the objectives of this thesis is to perform characterization of the materials synthesised using advanced techniques such as X-Ray Diffractometer (XRD), Field Emission Scanning Electron Microscope (FESEM), X-Ray Photoelectron Spectroscopy (XPS), Transmission Electron Microscope (TEM) and other sophisticated instruments.

References:

1. Newton, Marshall D., et al. "Electron transfer in chemistry ." (2001).
2. ArnulfJager-Waldau, Solar Energy Materials and Solar Cells, Volume 95, Issue 6, June 2011, Pages 1509-1517
3. K. Aryal, B. N. Pantha, J. Li, J. Y. Lin, and H. X. Jiang, Applied Physics Letters 96, 052110 (2010)
4. Ludmila P. Oleksenko, Nelly P. Maksymovych, Evgeniy V. Sokovykh, Igor P.

Matushko, Andrii I. Buvailo, Norman Dollahon, Sensers and Actuators B 196 (2014) 298-305

5. A. Ohtomo, M. Kawasaki, T. Koida, K. Masubuchi, H. Koinuma, Y. Sakurai, Y. Yoshida, T. Yasuda, and Y. Segawa, Applied Physics Letters 72, 2466 (1998)
6. Ryu Abe, Kazuhiro Sayama, and Hideki Sugihara, J. Phys. Chem. B 2005, 109, 16052-16061
7. Nanostructures and Nanomaterials: Synthesis, Properties and Applications; Guozhong Cao.
8. https://www.nano.gov/nanotech-101/what/ definition.
9. Journal of Faculty of Engineering & Technology, 2007, 2008, pages, 1120.
10. Introduction to Nanoscience, Kai Nordlund 2005.
11. P. Motiarty, Rep. Prog. Phys. 64 (2001) 297.
12. Sinha, Tridib Kumar. "Morphology-dependent visible light photocatalysis." *Nanostructured Materials for Visible Light Photocatalysis*. Elsevier, 2022. 375-412.
13. Kuo-Feng Lin, Hsin-Ming Cheng, Hsu-Cheng Hsu, Li-Jiaun Lin, Wen-Feng Hsieh, Chemical Physics Letters 409 (2005) 208-211
14. O. Vigil, F. Cruz, A. Morales-Acevedob, G. Contreras-Puente, Materials Chemistry and Physics 68 (2001) 249-252
15. G. Anil Kumar, M. V. Ramana Reddy, KattaNarasimha Reddy, Journal of Physics: Conference Series 365 (2012) 012031
16. H. Merzouk, A. Chelouche, S. Saoudi, D. Djouadi, A. Aksas, ApplPhys A (2012) 109: 841-844
17. B. SrinivasaRao, V. Rajagopal Reddy, B. Rajesh Kumar, T. SubbaRao, International Journal of Nanoscience, Vol. 11, No. 3 (2012) 1240006(5pages)
18. SoumenDhara, P. K Giri, Journal of Experimental Nanoscience, 8(2013) 3, 332-340.

19. C. Suryanarayana, Bull. Mater. Sci., 17 (1994) 307
20. G. A. Ozin and A. C. Arsenault, Nanochemistry, RSC Publishing,Cambridge,UK, 2005.
21. H. W. Kroto, J. R. Heath, S. C. O'Brien, R. F. Curl and R. E. Smalley, Nature, 1985, 318, 162–163.
22. S. Iijima, Nature, 1991, 354, 56–58.
23. K. S. Novoselov, A. K. Geim, S. V. Morozov, D. Jiang, Y. Zhang, S. V. Dubonos, I. V. Grigorieva and A. A. Firsov, Science, 2004, 306, 666–669.
24. Gomez-Navarro, M. B. C., J. Gomez-Herrero, and F. Zamora. "2D materials: To graphene and beyond." *Nanoscale* 3.1 (2011): 20.
25. Novoselov KS, Geim AK, Morozov SV, Jiang D, Zhang Y, Dubonos SV, et al.Electric field effect in atomically thin carbon films. Science 2004;306:666e9.
26. Allen MJ, Tung VC, Kaner RB. Honeycomb carbon: a review of graphene. Chem Rev 2010;110:132e45.
27. Soldano C, Mahmood A, Dujardin E. Production, properties and potential of graphene. Carbon 2010;48:2127e50.
28. Bae S, Kim H, Lee Y, Xu X, Park JS, Zhang Y, et al. Roll-to-roll production of 30- inch graphene films for transparent electrodes. Nat Nanotechnol 2010;5:574e8.
29. Zang X, Chen Q, Li P, He Y, Li X, Zhu M, et al. Highly flexible and adaptable, all-solid-state supercapacitors based on graphene wovenfabric film electrodes. Small 2014;10:2583e8.
30. Li X, Zang X, Li X, Zhu M, Chen Q, Wang K, et al. Hybrid heterojunction and solid-state photoelectrochemical solar cells. Adv Energy Mater 2014;4:1400224.
31. Li X, Xie D, Park H, Zeng Helen T, Wang K, Wei J, et al. Anomalous behaviors of graphene transparent conductors in graphene-silicon heterojunction solar cells. Adv Energy Mater 2014;3:1029e34.
32. Wang Y, Wang L, Yang T, Li X, Zang X, Zhu M, et al. Wearable and highly sensitive graphene strain sensors for human motion monitoring. Adv Funct Mater 2014;24:4666e70.
33. Ganatra R, Zhang Q. Few-layer MoS2: a promising layered semiconductor. ACS Nano 2014;8:4074e99.
34. Chhowalla M, Shin HS, Eda G, Li LJ, Loh KP, Zhang H. The chemistry of two- dimensional layered transition metal dichalcogenide nanosheets. Nat Chem 2014;5:263e75.

35. Geim AK, Grigorieva IV. van der Waals heterostructures. Nature 2013;499:419e25.
36. Yu GL, Jalil R, Belle B, Mayorov AS, Blake P, Schedin F, et al. Interaction phenomena in graphene seen through quantum capacitance. PNAS 2013;110:3282e6.
37. Wi S, Kim H, Chen M, Nam H, Guo LJ, Meyhofer E, et al. Enhancement of photovoltaic response in multilayer MoS2 induced by plasma doping. ACS Nano 2014;8:5270e81.
38. Ding S, Zhang D, Chen JS, Lou XW. Facile synthesis of hierarchical MoS2 microspheres composed of few-layered nanosheets and their lithium storageproperties. Nanoscale 2012;4:95e8.
39. Li Y, Wang H, Xie L, Liang Y, Hong G, Dai H. MoS2 nanoparticles grown on graphene: an advanced catalyst for the hydrogen evolution reaction. J Am Chem Soc 2011;133:7296e9.
40. Wu W, Wang L, Li Y, Zhang F, Lin L, Niu S, et al. Piezoelectricity of single-atomic-layer MoS2 for energy conversion and piezotronics. Nature 2014;514:470e4.
41. Jariwala D, Sangwan VK, Lauhon LJ, Marks TJ, Hersam MC. Emerging device applications for semiconducting two-dimensional transition metal dichalcogenides. ACS Nano 2014;8:1102e20.
42. Eda G, Yamaguchi H, Voiry D, Fujita T, Chen M, Chhowalla M. Photoluminescence from chemically exfoliated MoS2. Nano Lett 2011;11:5111e6.
43. Akinwande D, Petrone N, Hone J. Two-dimensional flexible nanoelectronics. Nat Commun 2014;5(5678):1e12.
44. Yang, D., S. J. Sandoval, W. M. R. Divigalpitiya, J. C. Irwin, and R. F. Frindt. 1991. Structure of single-molecular-layer MoS2. Phys. Rev. B 43:12053–12056.
45. Late, D. J., B. Liu, H. S. S. R. Matte, V. P. Dravid, and C. N. R. Rao. 2012. Hysteresis in single-layer MoS2 field effect transistors. ACS Nano 6:5635–5641.
46. Ataca, C., M. Topsakal, E. Aktürk, and S. Ciraci. 2011. A comparative study of lattice dynamics of three-and two-dimensional MoS2. J. Phys. Chem. C 115:16354–16361.
47. Ataca, C., H. S¸ahin, and S. Ciraci. 2012. Stable, single-layer MX2 transition-metal oxides and dichalcogenides in a honeycomb-like structure. J. Phys. Chem. C 116:8983–8999.
48. Beal, A. R., J. C. Knights, and W. Y. Liang. 1972. Transmission spectra of some transition metal dichalcogenides. II. Group via: trigonal prismatic coordination. J. Phys. C: Solid State Phys. 5:3540.

49. Shirodkar, S. N., and U. V. Waghmare. 2014. Emergence of ferroelectricity at a metal-semiconductor transition in a 1T monolayer of MoS2. Phys. Rev. Lett. 112:157601.
50. Acerce, M., D. Voiry, and M. Chhowalla. 2015. Metallic 1t phase MoS2 nanosheets as supercapacitor electrode materials. Nat. Nanotechnol. 10:313–318.
51. Cheng, P., K. Sun, and Y. H. Hu. 2016. Memristive behavior and ideal memristor of 1T phase MoS2 nanosheets. Nano Lett. 16:572–576.
52. Cheng, P., K. Sun, and Y. H. Hu. 2016. Mechanically-induced reverse phase transformation of MoS2 from stable 2H to metastable 1T and its memristive behavior. RSC Adv. 6:65691–65697.
53. Kuc, A. 2015. Low-dimensional transition-metal dichalcogenides. Pp. 1–29 *in* M. Springborg, and J. Joswig, ed. Chemical modelling: volume 11. The Royal Society of Chemistry, London, UK.
54. Novoselov, K. S., D. Jiang, F. Schedin, T. J. Booth, V. V. Khotkevich, S. V. Morozov, et al. 2005. Two-dimensional atomic crystals. Proc. Natl Acad. Sci. USA 102:10451–10453.
55. Li, H., Z. Yin, Q. He, H. Li, X. Huang, G. Lu, et al. 2012. Fabrication of single-and multilayer MoS2 film-based field-effect transistors for sensing no at room temperature. Small 8:63–67.
56. Coleman, J. N., et al. 2011. Two-dimensional nanosheets produced by liquid exfoliation of layered materials. Science 331:568–571.
57. Zhou, K.-G., N.-N. Mao, H.-X. Wang, Y. Peng, and H.-L. Zhang. 2011. A mixed-solvent strategy for efficient exfoliation of inorganic graphene analogues. Angew. Chem. Int. Ed. 50:10839–10842.
58. Wang, X., H. Feng, Y. Wu, and L. Jiao. 2013. Controlled synthesis of highly crystalline MoS2 flakes by chemical vapor deposition. J. Am. Chem. Soc. 135:5304– 5307.
59. Huang, X., Z. Zeng, and H. Zhang. 2013. Metal dichalcogenide nanosheets: preparation, properties and applications. Chem. Soc. Rev. 42:1934–1946.
60. Ramakrishna Matte, H. S. S., A. Gomathi, A. K. Manna, D. J. Late, R. Datta, S. K. Pati, et al. 2010. MoS2 and WS2 analogues of graphene. Angew. Chem. Int. Ed. 49:4059–4062.
61. Altavilla, C., M. Sarno, and P. Ciambelli. 2011. A novel wet chemistry approach for the synthesis of hybrid 2D free-floating single or multilayer nanosheets of MS2@ Oleylamine (M=Mo, W). Chem. Mater. 23:3879–3885.

CHAPTER 2

INTRODUCTION TO HER

2.1 Introduction to Hydrogen Evolution Reaction (HER)

There has been significant worldwide concern over environmental degradation, the phenomenon of global warming, and the energy crisis resulting from extensive use of fossil fuels [1]. In order to effectively mitigate environmental and energy-related challenges, it is essential to priorities the advancement of sustainable and renewable energy sources, with the development of efficient energy storage and conversion technologies. The combination of grid-scale renewable energy harvesting technologies with electrochemical water splitting emerges as a very promising strategy. Moreover, hydrogen is often regarded as the most efficient means of transporting clean energy because to its exceptional mass-energy density, surpassing that of any other fuel.

The identification of inexpensive, exceptionally efficient, and durable catalysts for hydrogen evolution reactions (HERs) is of utmost importance in order to effectively implement the process of water splitting. The remarkable electrocatalytic capabilities of heterostructure catalysts, composed of electrochemically active materials and diverse functional additives, have recently been shown in their ability to facilitate the hydrogen evolution reaction (HER). Several heterostructures that do not include precious metals exhibited similar levels of activity compared to catalysts that do contain precious metals.

In a typical water electrolysis setup, the hydrogen evolution reaction (HER) occurs at the cathode. These reactions result in the production of hydrogen gas (H2). To overcome the energy barrier of the process, which is around 237 kJ mol-1, an external current is applied. Platinum (Pt) now stands as the catalyst with the highest level of advancement for the hydrogen evolution reaction (HER), whilst catalysts based on noble metals remain the most efficient catalysts for both HER [2-5]. Hence, a primary focus in advancing the progress of cost-effective and efficient water electrolysis systems is in the development of catalysts that exhibit elevated activity levels and are composed of readily available elements.

Several catalysts that are common on Earth have been discovered so far [6–13], and they exhibit notable catalytic activity in the hydrogen evolution reaction (HER). Extensive study has been conducted on the topic of hydrogen evolution reaction (HER) in connection to transition metal dichalcogenides (TMDs), transition metal phosphides (TMPs), carbides, [24–26], and nitrides [27, 28]. In recent times, a variety of heterostructured catalysts have shown their superiority over other catalysts by exhibiting enhanced catalytic performance in the context of electrochemical water splitting [29–33].

2.2 Mechanisms of Electrochemical HER

Reduction-oxidation (redox) reactions occur at the interface between the electrode and electrolyte in the context of electrocatalytic hydrogen evolution reaction (HER), which fundamentally represents an electrochemical process. Hydrogen gas (H2) may be generated by two distinct mechanisms: the reduction of protons (H+) or the reduction of water (H2O). These processes are influenced by several basic factors, such as the pH level of the electrolyte.

2.2.1 HER in Acidic Media

The occurrence of the hydrogen evolution reaction (HER) in acidic conditions at the surface of various catalysts is generally known [34-36]. At the beginning of the hydrogen evolution process (HER), a hydrogen ion (H+) undergoes adsorption to generate an adsorbed hydrogen atom (H*), with the asterisk symbol (*) indicating an active site located on the surface of the catalyst. The technique described in Equation (1) is often referred to in academic literature as the Volmer step or discharge step.

The Heyrovsky step, alternatively referred to as the electrochemical desorption step, involves the combination of a hydrogen atom (H*) with a hydrogen ion (H+), an electron (e), and a hydrogen molecule (H2), as seen in Equation (2). An alternative approach to generate hydrogen (H2) is by means of the Tafel step, often referred to as the chemical desorption step. This process entails the combination of two hydrogen atoms (H*) on the surface of the catalyst, as represented by Equation 3. Equation (4) depicts the comprehensive reaction of the hydrogen evolution reaction (HER) [37], using the standard electrode potential (E°) as a reference point for evaluating the standard electrode potential of electrochemical processes. According to the Sabatier principle [38], the kinetics of the hydrogen evolution reaction (HER) are significantly influenced by the contact between the catalyst and H*[39].

- Acidic media:

$$H^+ + e^- \rightarrow H^* \quad (1)$$

$$H^* + H^+ + e^- \rightarrow H_2 \quad (2)$$

$$2H^* \rightarrow H_2 \quad (3)$$

$$2H^+ + 2e^- \rightarrow H_2 \quad (4)$$

2.2.2 HER in Alkaline Media

In relation to the hydrogen evolution reaction (HER) in alkaline environments, previous studies have shown that the exchange current densities in alkaline solutions are often much lower, by two to three orders of magnitude, compared to acidic electrolytes [40, 41]. One of the primary contributors to the diminished catalytic activity is the divergence in the route of the alkaline hydrogen evolution reaction (HER) compared to its acidic counterpart. In the absence of H+ ions, the hydrogen evolution reaction (HER) in alkaline environments initiates via the dissociation of water molecules, resulting in the generation of protons. The process described is engaged in both the Volmer step (Equation 5) and the Heyrovsky step (Equation 6) of alkaline hydrogen evolution reaction (HER), whereas the Tafel step remains unchanged compared to acid solutions. The overall reaction mechanism is described by Equation (7), and the standard electrode potential (E0) of the reaction with respect to the standard hydrogen electrode (SHE) is -0.826 V.

The kinetics of the hydrogen evolution reaction (HER) on most catalysts exhibits a reduced rate in alkaline electrolytes due to the higher energy need for proton generation in an alkaline environment. The activity of alkaline hydrogen evolution reaction (HER) is said to be controlled by a delicate balance between the standard Gibbs free energy change (ΔGH°) and the energy required for the dissociation of water [36]. The catalysts MoS2 and Co2P have been shown to be less favorable for the process of water dissociation, as indicated by previous studies [42, 43]. Therefore, an effective approach for developing efficient catalysts for alkaline hydrogen evolution reaction (HER) involves promoting the dissociation of water while simultaneously retaining a modest level of hydrogen adsorption energy.

- Alkaline media:

$$H_2O + e^- \rightarrow H^* + OH^- \quad (5)$$

$$H^* + H_2O + e^- \rightarrow OH^- + H_2 \quad (6)$$

$$2H_2O + 2e^- \rightarrow 2OH^- + H_2 \quad (7)$$

2.3 Methods Generally Used for evaluating Catalytic Performance

2.3.1 Overpotential

Overpotential is one of the most important factors to consider when assessing a water splitting catalyst since a significant overpotential is what contributes to the electrochemical water electrolysis system's low energy conversion efficiency [35]. The overpotential of an electrochemical process is the discrepancy between the experimentally measured potential and the thermodynamically predicted potential. When doing linear sweep voltammetry (LSV), which is usually used to determine the overpotential, small sweep rates (such as 2 mV s-1 or 5 mV s-1) are frequently utilized to lower the nonfaradic current. Possible sources of the overpotential include reaction activation, charge carrier diffusion, and series resistance. To be more precise, the overpotentials caused by activation directly relate to catalytic activity, while those caused by series resistance and charge-carrier diffusion predominantly come from the water electrolysis system. Therefore, rigorous research should be done on the activation overpotential in order to more precisely measure the materials' catalytic activity. Using a rotate disc electrode (RDE) method, in which the electrode spins constantly while LSV curves are being recorded, may efficiently minimize the diffusion overpotential. In the interim, the resistance overpotential may be corrected using IR compensation (Equation (8)), where I is the circuit's current and Rs is the series resistance.

$$E_{corrected} = E_{uncorrected} - IR_S \quad (8)$$

The overpotential at 10 mA cm2, which corresponds to the working current density of the most commercially feasible photoelectrochemical water splitting system, has traditionally been used as a benchmark for assessing catalyst performance [44, 45]. The mass of the catalyst is commonly used to calculate the geometric area of the electrode, which may alternatively be calculated based on the specific geometric area of the catalyst, the specific area of the catalyst that is electrochemically active, or both.

2.3.2 Tafel Slope and Exchange Current Density

Tafel slope is the slope of the linear section of a Tafel plot (overpotential vs. log |current density|), which may be created by replotting the corresponding LSV curve. Tafel slope, in particular, may

provide light on the catalyst surface HER reaction process. The anticipated Tafel slope for the Volmer, Heyrovsky, and Tafel steps in HER is 120, 40, and 30 mV dec-1, respectively [34, 46]. For instance, the Tafel step is the rate-determining step (RDS) for the reaction when the Volmer-Tafel technique is applied, as shown by the HER on the surface of commercial Pt in 0.5 M H2SO4, which is close to 30mV dec-1 [47]. It is common to assume that H* has an extreme coverage (0 or 1) while analysing the RDS of HER using the Tafel slope. However, the Tafel slope is coverage-dependent. An too straightforward reading of the Tafel slope will lead to an incorrect representation of the response [48]. The exchange current density of a reaction is the current density at the equilibrium potential, when the cathodic current and the anodic current are equal [35]. It may be found by observing the intersection of the projected linear part of the Tafel plots with the X-axis. Promoting the exchange current density is akin to catalysing a reaction since it essentially represents the intrinsic activity of charge transfer between electrode and electrolyte [49]. Catalyst surfaces with greater catalytic activity often have denser exchange currents. To provide an example, in 0.5 M H2SO4, the current densities of HER on the surfaces of Pt, Ti, and Hg are around 1, 10-5, and 10-9 mA cm-2, respectively [50].

2.3.3 Turnover Frequency

The turnover frequency (TOF), defined by Equation (9) [51, 52], is the number of product molecules created by an active site per unit of time. According to the definition, H2 should be obtained to count the molecules. When the Faradic efficiency is assumed to be 100%, the theoretical amount of H2 can be calculated from the charge moving through the circuit using Faraday's laws of electrolysis (Equation 10), where n is the amount of substance (mol), I is current (A), z is the number of electrons transferred per molecule, and F is the Faraday constant (96485 C mol-1). The TOF vs. overpotential curve is then represented by Equation (11), which was created by combining Equations (9) and (10) before. The number of active sites must be known in order to calculate TOF. This could be a number of methods, including the copper underpotential deposition method [14], the counting of molecules on the exposed surface [53–55], and the quantification from cyclic voltammetry (CV) tests. Evidently, whether a realistic TOF or TOF-overpotential curve can be created depends on how the number of active sites is defined and evaluated. It is highlighted that the overpotential value should always be provided when reporting the TOF data since TOF rises with growing overpotentials.

$$TOF = \frac{\text{molecule number of product}}{n\text{umber of active sites}} \times \frac{1}{unit\ time} \quad (9)$$

$$n = \frac{I_t}{zF} \quad (10)$$

$$TOF = \frac{I \times n_A}{zF \times number\ of\ active\ site} \quad (11)$$

2.3.4 Stability

The ability of a catalyst to maintain its initial activity over a lengthy period of time is shown by its stability or durability, which is a critical characteristic in terms of practical usage. The stability may be determined by examining the fluctuation in the applied overpotential at a certain current density or the evolution of the cathodic current density at an applied overpotential over time. Additionally, continuous CV cycling may be utilized to rate it. Since LSV curves are often taken before and after the stability test, the overpotential will be noticeably raised if the catalyst loses its activity soon. It should be highlighted that there are no trustworthy techniques for evaluating stability in inactive settings, and the present approaches focus on measuring stability in active situations.

Reference:

1. S. Chu, A. Majumdar, *Nature* **2012**, *488*, 294.
2. P. Wang, X. Zhang, J. Zhang, S. Wan, S. Guo, G. Lu, J. Yao, X. Huang, Nat. Commun 2017, 8, 14580.
3. J. Lim, D. Park, S. S. Jeon, C.-W. Roh, J. Choi, D. Yoon, M. Park, H. Jung, H. Lee, Adv. Funct. Mater. 2018, 28, 1704796.
4. J. Ying, G. Jiang, Z. P. Cano, L. Han, X.-Y. Yang, Z. Chen, Nano Energy 2017, 40, 88.
5. L. Zhang, L. Han, H. Liu, X. Liu, J. Luo, Angew. Chem., Int. Ed. 2017, 56, 13694.
6. Y. Zhang, Q. Zhou, J. Zhu, Q. Yan, S. X. Dou, W. Sun, *Adv. Funct. Mater.* **2017**, *27*, 1702317.
7. H. Fan, H. Yu, Y. Zhang, Y. Zheng, Y. Luo, Z. Dai, B. Li, Y. Zong, Q. Yan, *Angew. Chem.* **2017**, *129*, 12740.
8. J. X. Feng, L. X. Ding, S. H. Ye, X. J. He, H. Xu, Y. X. Tong, G. R. Li, *Adv. Mater.***2015**, *27*, 7051.
9. H. Cheng, C.-Y. Su, Z.-Y. Tan, S.-Z. Tai, Z.-Q. Liu, *J. Power Sources* **2017**, *357*, 1.
10. G. F. Chen, T. Y. Ma, Z. Q. Liu, N. Li, Y. Z. Su, K. Davey, S. Z. Qiao, *Adv. Funct. Mater.* **2016**, *26*, 3314.
11. H. Cheng, Y.-Z. Su, P.-Y. Kuang, G.-F. Chen, Z.-Q. Liu, *J. Mater. Chem. A* **2015**, *3*, 19314.
12. D. Yan, Y. Li, J. Huo, R. Chen, L. Dai, S. Wang, *Adv. Mater.* **2017**, *29*, 1606459.
13. A.-L. Wang, H. Xu, G.-R. Li, *ACS Energy Lett.* **2016**, *1*, 445.
14. D. Voiry, H. Yamaguchi, J. Li, R. Silva, D. C. Alves, T. Fujita, M. Chen, T. Asefa, V.B. Shenoy, G. Eda, M. Chhowalla, *Nat. Mater* **2013**, *12*, 850.
15. Y. Kim, D. H. Jackson, D. Lee, M. Choi, T. W. Kim, S. Y. Jeong, H. J. Chae, H. W. Kim, N. Park, H. Chang, *Adv. Funct. Mater.* **2017**, *27*, 1701825.
16. C. Xu, S. Peng, C. Tan, H. Ang, H. Tan, H. Zhang, Q. Yan, *J. Mater. Chem. A* **2014**,*2*, 5597.
17. C. Ouyang, X. Wang, S. Wang, *Chem. Commun.* **2015**, *51*, 14160.
18. L. Tao, X. Duan, C. Wang, X. Duan, S. Wang, *Chem. Commun.* **2015**, *51*, 7470.
19. J.-X. Feng, J.-Q. Wu, Y.-X. Tong, G.-R. Li, *J. Am. Chem. Soc.* **2018**, *140*, 610.
20. D. Y. Chung, S. W. Jun, G. Yoon, H. Kim, J. M. Yoo, K. S. Lee, T. Kim, H. Shin, A.K. Sinha, S. G. Kwon, K. Kang, T. Hyeon, Y. E. Sung, *J. Am. Chem. Soc.* **2017**, *139*,6669.
21. J. Zhang, T. Wang, P. Liu, S. Liu, R. Dong, X. Zhuang, M. Chen, X. Feng, *Energy*

Environ. Sci. **2016**, *9*, 2789.

22. Z. Zhang, B. Lu, J. Hao, W. Yang, J. Tang, *Chem. Commun.* **2014**, *50*, 11554.
23. A.-L. Wang, J. Lin, H. Xu, Y.-X. Tong, G.-R. Li, *J. Mater. Chem. A* **2016**, *4*, 16992.
24. C. Wan, Y. N. Regmi, B. M. Leonard, *Angew. Chem.* **2014**, *126*, 6525.
25. H. Ang, H. T. Tan, Z. M. Luo, Y. Zhang, Y. Y. Guo, G. Guo, H. Zhang, Q. Yan,*Small* **2015**, *11*, 6278.
26. H. Ang, H. Wang, B. Li, Y. Zong, X. Wang, Q. Yan, *Small* **2016**, *12*, 2859.
27. W. F. Chen, K. Sasaki, C. Ma, A. I. Frenkel, N. Marinkovic, J. T. Muckerman, Y. Zhu, R. R. Adzic, *Angew. Chem., Int. Ed.* **2012**, *51*, 6131.
28. H. Yan, C. Tian, L. Wang, A. Wu, M. Meng, L. Zhao, H. Fu, *Angew. Chem., Int. Ed.* **2015**, *54*, 6325.
29. H. Lin, Z. Shi, S. He, X. Yu, S. Wang, Q. Gao, Y. Tang, *Chem. Sci.* **2016**, *7*, 3399.
30. D. Wang, Q. Li, C. Han, Z. Xing, X. Yang, *ACS Cent. Sci.* **2017**, *4*, 112.
31. K. Rui, G. Zhao, Y. Chen, Y. Lin, Q. Zhou, J. Chen, J. Zhu, W. Sun, W. Huang, S. X. Dou, *Adv. Funct. Mater.* **2018**, *28*, 1801554.
32. S. Dou, J. Wu, L. Tao, A. Shen, J. Huo, S. Wang, *Nanotechnology* **2015**, *27*, 045402.
33. Y. Chen, Q. Zhou, G. Zhao, Z. Yu, X. Wang, S. X. Dou, W. Sun, *Adv. Funct. Mater.***2018**, *28*, 1705583.
34. B. Conway, B. Tilak, *Electrochim. Acta* **2002**, *47*, 3571.
35. A. J. Bard, L. R. Faulkner, J. Leddy, C. G. Zoski, *Electrochemical Methods: Fundamentals and Applications*, Wiley, New York **1980**.
36. N. Danilovic, R. Subbaraman, D. Strmcnik, V. R. Stamenkovic, N. M. Markovic, *J. Serb. Chem. Soc.* **2013**, *78*, 2007.
37. H. Lehmann, X. Fuentes-Arderiu, L. Bertello, *Pure Appl. Chem.* **1996**, *68*, 957.
38. P. Quaino, F. Juarez, E. Santos, W. Schmickler, *Beilstein J. Nanotechnol.* **2014**, *5*, 846.
39. R. Parsons, *Trans. Faraday Soc.* **1958**, *54*, 1053.
40. N. Danilovic, R. Subbaraman, D. Strmcnik, K. C. Chang, A. P. Paulikas, V. R. Stamenkovic, N. M. Markovic, *Angew. Chem., Int. Ed. Engl.* **2012**, *51*, 12495.
41. T. Schmidt, P. Ross, N. Markovic, *J. Electroanal. Chem.* **2002**, *524*, 252
42. K. Xu, H. Ding, M. Zhang, M. Chen, Z. Hao, L. Zhang, C. Wu, Y. Xie, *Adv. Mater.***2017**, *29*, 1606980.
43. K. K. Ghuman, S. Yadav, C. V. Singh, *J. Phys. Chem. C* **2015**, *119*, 6518.
44. J. Luo, J.-H. Im, M. T. Mayer, M. Schreier, M. K. Nazeeruddin, N.-G. Park, S. D.

Tilley, H. J. Fan, M. Gratzel, *Science* **2014**, *345*, 1593.

45. J. D. Benck, T. R. Hellstern, J. Kibsgaard, P. Chakthranont, T. F. Jaramillo, *ACS Catal.* **2014**, *4*, 3957.
46. A. R. Kucernak, C. Zalitis, *J. Phys. Chem. C* **2016**, *120*, 10721.
47. Y. Li, H. Wang, L. Xie, Y. Liang, G. Hong, H. Dai, *J. Am. Chem. Soc.* **2011**, *133*, 7296.
48. T. Shinagawa, A. T. Garcia-Esparza, K. Takanabe, *Sci. Rep.* **2015**, *5*, 13801.
49. C. H. Hamann, A. Hamnett, W. Vielstich, Weinheim, *Electrochemistry*, 2nd ed., Wiley-VCH, Weinheim **2007**.
50. C. Cao, *Principles of Electrochemistry of Corrosion*, Chem. Ind. Press, Peking, China 2008.
51. J. M. Thomas, W. J. Thomas, *Principles and Practice of Heterogeneous Catalysis*, John Wiley & Sons, Weinheim **2014**.
52. C. Costentin, S. Drouet, M. Robert, J. M. Saveant, *J. Am. Chem. Soc.* **2012**, *134*, 11235.
53. H. Li, C. Tsai, A. L. Koh, L. Cai, A. W. Contryman, A. H. Fragapane, J. Zhao, H. S. Han, H. C. Manoharan, F. Abild-Pedersen, *Nat. Mater.* **2016**, *15*, 48
54. S. Shin, Z. Jin, D. H. Kwon, R. Bose, Y. S. Min, *Langmuir* **2015**, *31*, 1196.
55. J. Kibsgaard, T. F. Jaramillo, F. Besenbacher, *Nat. Chem.* **2014**, *6*, 248.

Chapter 3

LITERATURE REVIEW OF PAST WORK

3.1 General Idea:

The overuse of traditional fossil fuels and the exponentially rising demand for energy are hastening their depletion, and rising carbon emissions are also having a negative impact on the environment. Alternative (cheap and green) energy solutions are urgently needed in the present situation to better meet these needs. Green hydrogen has zero carbon emissions, is recyclable, has a high conversion efficiency, and has a high energy density, making it a dependable alternative to conventional fossil fuels. By 2025 and 34% by 2050, hydrogen is expected to contribute 11% and 34%, respectively, of the world's total energy requirements. Currently, carbon dioxide emissions from the steam methane reforming of natural gas used to make hydrogen are produced on an industrial scale. However, because hydrogen is created using renewable energy sources, electro- and photocatalytic water splitting are favoured.2 Due to their optimal absorption and binding energies for hydrogen and protons, precious noble metals including ruthenium (Ru), iridium (Ir), palladium (Pd), and platinum (Pt), as well as their alloys, are the most effective catalysts for electrocatalytic and photocatalytic water splitting. However, natural scarcity and the ensuing high price of such metals restrict their use.3 As effective HER catalysts, transition metal-based compounds have recently attracted interest.4 Due to their tunable properties, two-dimensional (2D) earth-abundant transition metal dichalcogenides (TMDCs) are chosen among them. Extensive research has been conducted on the efficacy of MoS2 as a catalyst for the hydrogen evolution reaction (HER). Nevertheless, empirical investigations have shown that MoSe2 exhibits more favorability owing to its heightened metallic characteristics, reduced Gibbs free energy, and shorter band gap.The numerical expression 8-10 can be simplified to -2. The catalytic performance of MoSe2 is heavily influenced by the presence of edge sites and its overall shape.The numerical value provided by the user is 8. Furthermore, the narrow energy band gap and capacity to function as an electron donor in bicatalytic systems establish MoSe2 as a dependable cocatalyst for the process of water photolysis.The numbers 8 and 11 are being referenced. However, researchers are motivated to enhance the hydrogen evolution reaction (HER) performance of MoSe2 due to some limitations, such as lower conductivity compared to noble metal catalysts and the tendency of MoSe2 to aggregate during manufacturing. Consequently, various strategies are being explored to address these shortcomings and further enhance the HER performance of MoSe2.

3.2 Synthesis and Characterization of $MoSe_2$

The synthesis of MoSe2 presents challenges in following conventional reaction paths because to the significant disparity in the melting temperatures of Mo and Se atoms [1]. One of the primary obstacles encountered in the synthesis of MoSe2 is the use of solid selenium, which exhibits lower reactivity and hence necessitates the presence of a reductant. Hence, many diverse synthetic approaches are used for the synthesis of the compound, which will be briefly discussed in the next section.

3.2.1 Hydrothermal Process

The hydrothermal approach is widely used as the predominant technique for the creation of MoSe2 nanostructures. In this methodology, water is used as the solvent for the purpose of dissolving and then reforming the precursor materials at elevated pressure and temperature conditions. This process is typically conducted at temperatures over 100°C inside a Teflon-lined autoclave. Consequently, the resulting crystals exhibit a reduced number of inherent flaws and enhanced thermal stability, as shown by previous research [2]. The reaction occurs in the presence of strong reducing agents such as hydrazine and NaBH4 [3,4]. For example, $MoSe_2$ nanoflowers (NF) were synthesised by a hydrothermal method involving the use of $Na2MoO_4.2H_2O$ and N_2H_4 solution containing Se and NaBH4. The synthesis process included heating the mixture at a temperature of 200°C for a duration of 48 hours in an autoclave [5,6]. The elevated temperature induces the breakdown of N_2H_4, resulting in the formation of ammonia (NH_3), hydrogen gas (H_2), and nitrogen gas (N_2). Hydrogen (H_2) and nitrogen (N_2) were used as reducing agents in conjunction with the significant presence of ammonia (NH_3) to effectively prevent the stacking of $MoSe_2$ layers, hence facilitating the synthesis of nitrogen-doped fluorine (NF). The aforementioned methodology has shown to be a viable strategy for synthesising $MoSe_2$ as a co-catalyst, resulting in the formation of various morphologies including broom-shaped [7] and micro-sphere [8] nanostructures of $MoSe_2$. The hydrothermal approach was used for the development of the materials. $Na_2MoO_4.2H_2O$ was used as the precursor for molybdenum, while immaculate Se powder was utilised in combination with N_2H_4 for selenium.The H_2O molecule functions as the reducing agent. One of the main obstacles in the production process of $MoSe_2$ is the insolubility of selenium. However, this issue has been addressed by including selenium cyanoacetic acid sodium as the source of selenium [9]. The method for the generation of $MoSe_2$ microspheres was facilitated by the high solubility of $NCSeCH_2COONa$, allowing for the use of ethylene glycol instead of hydrazine. This substitution of solvents resulted in a more environmentally friendly approach to the reaction.

3.2.2 Solvothermal process

The solvothermal synthesis approach is an expanded version of the hydrothermal process, characterised by the use of a non-aqueous solvent and a wider range of temperatures [3,10]. The use of an organic reaction medium is very advantageous in manipulating the shape of $MoSe_2$ nanostructures and expanding the range of reactions that are otherwise unfeasible under standard circumstances. For example, in this study, uniform platelet-shaped crystals of $MoSe_2$ were synthesised using MoO_3 as the precursor. The reduction of MoO_3 to MoO_2 was facilitated by the presence of Se, with N_2H_4 serving as the reducing agent. Pyridine was used as the solvent throughout the synthesis process. The resulting crystals were then analysed at various temperature ranges, as reported in reference [11]. The experiment was conducted for a duration of 12 hours at the appropriate temperature, which was found to fall between the range of 250 to 300 degrees Celsius. The resulting product exhibited an amorphous nature at low temperature conditions, whereas the degradation of pyridine was seen at elevated temperatures. Nevertheless, this methodology is not just limited to liquids or viscous substances, but may also be used to solids. In the case of solids, the precursors (namely MoO_3 and Se powder, together with hydrazine) were cultivated on a substrate made of carbon fibre fabric. This process included the utilisation of NH_4F additive. The nano-sheets that were obtained demonstrated a robust adhesion to the carbon cloth, consequently augmenting the efficiency of charge transfer during the process of photocatalytic water splitting. The experiment included monitoring the reaction across time intervals of 6, 9, and 12 hours, while maintaining a constant temperature of 220°C. The results indicated that as the reaction time increased, the number of spheres formed decreased, leading to a reduction in the catalytic activity of the nano-sheets.

Furthermore, the observed reaction took place in the absence of NH_4F, which implies that the utilisation of NH_4F is essential in order to control the excessive development of nano-sheets.

3.2.3 Chemical vapor deposition process

Chemical vapour deposition (CVD) is an alternative bottom-up technique used for the fabrication of $MoSe_2$ thin nanolayers. The process described entails the dilution of components in order to generate gaseous molecules, known as precursors. These precursors are then converted into solid thin layers on the substrate's surface by thermal decomposition in the presence of additional gases and liquids [12-14]. The growth mechanism of the CVD method varies for each synthesis process, since it is influenced by factors such as substrate characteristics, temperature, and atomic gas flow [5]. The optimisation of crystal shape may be achieved by modifying different parameters. In this study, $MoSe_2$ nano-ribbons were synthesised using MoO_3 and Se solids as precursors, and SiO_2/Si wafers as substrates. The synthesis process included the presence of a carrier gas mixture (H_2/Ar) [13]. The primary function of H_2, in conjunction with Se, is to provide a conducive atmosphere that facilitates the reduction process of MoO_3 to MoO(3-x), ultimately resulting in the formation of MoSe2 [12]. The study investigated the effect of varying H_2 content on morphology changes. Specifically, when the H_2 flow rate was set at 3 standard cubic centimetres per minute (sccm), $MOSe_2$ nanoplates were seen. As the H_2 concentration was raised to 4 sccm, these nanoplates exhibited a tendency to approach monolayer formation [13].

3.2.4 Intercalation and exfoliation

The effective production of $MoSe_2$ nanostructures using the exfoliation and intercalation technique is made possible by the presence of strong in-plane covalent bonding and weak interlayer van der Waal attraction [14]. The three-dimensional wave function of the mass becomes confined to a two-dimensional state due to the arrangement of nanosheets. The production of nanolayers/nanosheets by this synthetic procedure involves ion intercalation, liquid exfoliation, or a physical method utilising scotch tape. However, the process of liquid phase intercalation yields a superior nano sheet without causing any structural harm. This method is used for the purpose of large-scale manufacturing. On the other hand, ion exfoliation only allows for small-scale synthesis. As an example, the use of ultrasonication on a large quantity of $MoSe_2$ in solvents such as cyclohexyl pyrrolidone and N-methyl 2 pyrrolidone led to the formation of nanosheets consisting of either a single layer or several layers [15]. In addition, $MoSe_2$ monolayers were generated using Li intercalation using n-butyl lithium in hexane at temperatures of 60°C for a duration of 18 hours or 20°C for a period of 14 days [16]. Throughout the synthesis process, a pH level of 7 was

consistently maintained by using a continuous washing technique using de-ionized water. However, in addition to n-butyl lithium, tertiary butyl lithium was also used in the synthesis of 1 T $MoSe_2$ from 2H, as seen in Figure 4d [17]. As a result, the activation of the 1 T step occurs by the transfer of charge from lithium-ion to molybdenum Di selenide ($MoSe_2$) [18-22]. Nevertheless, the additional charge on $MoSe_2$ will experience stabilisation due to the alignment of nearby atoms, leading to a phase change from the 2H phase to the 1T phase. The residual negative charge is effectively balanced by the interaction with water molecules or the presence of any remaining Li-ions.

Catalyst	**current density (mA/cm2)**	**Overpotential (mV)**	**Tafel slope (mV/dec)**	**underlying mechanism for performance enhancement**	**ref**
interlayer-expanded 1T-MoSe2	10	179	78	2H → 1T phase transformation and layer expansion resulting in a lower Gibbs free energy for Hadsorption/desorption and anincreased number of active sites	23
2H-MoSe2	10	558	141		24
Plasma	10	148	51.6	more optimized active sites owing to Se vacancies and holes created through etching	25
etched MoSe2 (at 20W) 1T-$MoSe_2$ $MoSe_2$-4-180 ($MoSe_2$-x-T, x = $NaBH_4$: $Na_2MoO_4{\cdot}2H_2O$, T= temperature	10	152	52	2H → 1T phase transformation coupled with defect formation leading to increased intrinsic activity and more unsaturated Se active sites, respectively	26

°C)					
$MoSe_2$-1-180	10	148	51.6		27
$MoSe_2$-1-140	10	152	52		28
$MoSe_2$-4-160	10	355	146		29
$MoSe_2$-4-200	10	211	72		30
Pt	10	197	54		31
Defect-rich exfoliated $MoSe_2$	10	163	55	Structural defects, multiple Se vacancies, $MoSe_2$ andesite point defect,	32
bulk $MoSe_2$	10		30		33
Ni-doped $MoSe_2$	10	350	90	Ni−dopant-induced active sites and lower charge transfer resistance.	34
$MoSe_2$ nanosheets	10		150		35
$MoSe_2$/N-doped carbon	10	184	83	optimized adsorption and desorption of H* due to N-doped carbon confinement.	36
$MoSe_2$	10	335	118		37
N-doped carbon	10	162	62		38
Pt/C	10	468	164		39
$MoSe_2$−NiSe epitaxial growth strategy	10	859	286	synergistic interaction between MoSe2 and NiSe and enhanced conductivity.	40
pure $MoSe_2$	10	33	34		41
$MoSe_2$ + NiSe mixture	10	210	56		42

$MoSe_2/MoO_2/Mo$	10	160	TOF: 5.6 s^{-1} at 250 mV	synergistic effect of combining abundant active sites of MoSe2 and improved conductivity across MoSe2/MoO2/Mo	43
$MoSe_2/Mo$	10	267	65.2		44
$MoSe_2/WS_2$	10	75	60	Rapid interface charge transport and increased edge active sites.	45
$MoSe_2$	10	112	136		46
WS_2	10	158	114		47

Table-1 Presents a comprehensive analysis of the performance of catalysts based on MoSe2 for the hydrogen evolution reaction (HER), along with an examination of the underlying mechanisms involved.

Reference:

1. A. Efthelthari, Appl. Mater. Today 8 (2017) 1–17
2. C.H. Ravikumar, G.V. Nair, S. Muralikrishna, D. Nagaraju, R.G. Balakrishna, Mater. Lett. 220 (2018) 133–135.
3. X. Wu, Y.-H. Wang, P.-L. Li, Z.-Z. Xiong, Superlattice. Microst. 139 (2020)
4. T. Lu, S. Dong, C. Zhang, L. Zhang, G. Cui, Coord. Chem. Rev. 332 (2017) 75–99.
5. H. Tang, H. Huang, X. Wang, K. Wu, G. Tang, C. Li, Appl. Surf. Sci. 379 (2016) 296–303.
6. C.H. Ravikumar, G.V. Nair, S. Muralikrishna, D. Nagaraju, R.G. Balakrishna, Mater. Lett. 220 (2018) 133–135
7. W. Feng, W. Pang, Y. Xu, A. Guo, X. Gao, X. Qiu, W. Chen, ChemElectroChem 7 (2020) 31–54.
8. H. Tang, H. Huang, X. Wang, K. Wu, G. Tang, C. Li, Appl. Surf. Sci. 379 (2016) 296–303.
9. Y.-N. Zhou, Y.-R. Zhu, X.-Y. Chen, B. Dong, Q.-Z. Li, Y.-M. Chai, J. Alloy. Compd. 852 (2021)
10. Y. Hou, M.R. Lohe, J. Zhang, S. Liu, X. Zhuang, X. Feng, Energy Environ. Sci. 9 (2016) 478–483
11. J. Zhan, Z. Zhang, X. Qian, C.W.Y. Xie, Y. Qian, Mater. Res. Bull. 34 (1999) 497– 501.
12. J.C. Shaw, H. Zhou, Y. Chen, N.O. Weiss, Y. Liu, Y. Huang, X. Duan, Nano Res. 7 (2014) 511–517.
13. T. Chen, G. Hao, G. Wang, B. Li, L. Kou, H. Yang, X. Zheng, J. Zhong, 2D Materials 6 (2019).
14. Y. Li, F. Wang, D. Tang, J. Wei, Y. Li, Y. Xing, K. Zhang, Mater. Lett. 216 (2018) 261–264.
15. Shaffer, J.N. Coleman, ACS Nano 6 (2012) 3468–3480.
16. R. Gordon, D. Yang, E. Crozier, D. Jiang, R. Frindt, Phys. Rev. B 65 (2002).
17. N. Li, J. Wu, Y. Lu, Z. Zhao, H. Zhang, X. Li, Y.-Z. Zheng, X. Tao, Appl. Catal. B 238 (2018) 27–37.
18. Y. Zhao, J. Tu, Y. Sun, X. Hu, J. Ning, W. Wang, F. Wang, Y. Xu, L. He, J. Phys. Chem. C 122 (2018) 26570–26575.
19. H.-Y. He, Z. He, Q. Shen, Mater. Res. Bull. 111 (2019) 183–190.
20. K. Vasu, O.E. Meiron, A.N. Enyashin, R. Bar-Ziv, M. Bar-Sadan, J. Phys. Chem. C 123 (2018) 1987–1994.

21. F. Shi, C. Xing, X. Wang, Int. J. Hydrogen Energy 46 (2021) 38636–38644. [57] Y. Fan, J. Wang, M. Zhao, Nanoscale 11 (2019) 14836–14843.

22. B. Wang, X. Wang, P. Wang, T. Yang, H. Yuan, G. Wang, H. Chen, Nanomaterials 9 (2019) 1706. [59] H. Li, W. Tu, Y. Zhou, Z. Zou, Adv. Sci. 3 (2016) 1500389.

23. C.-F. Fu, X. Li, J. Yang, Chem. Sci. 12 (2021) 2863–2869.

24. V. Hasija, A. Kumar, A. Sudhaik, P. Raizada, P. Singh, Q. Van Le, T.T. Le, V.-H. Nguyen, Environ. Chem. Lett. 19 (2021) 2941–2966.

25. C. Zhu, Q. He, T. Sun, M. Xu, J. Wang, C. Chen, X. Duan, H. Xu, S. Wang, Chem. Eng. J. 464 (2023).

26. X. Wang, X. Wang, J. Huang, S. Li, A. Meng, Z. Li, Nat. Commun. 12 (2021) 1–11.

27. D. Gao, B. Xia, Y. Wang, W. Xiao, P. Xi, D. Xue, J. Ding, Small 14 (2018) 1704150. [65] C. Ding, C. Zhao, S. Cheng, X. Yang, Surf. Interfaces 25 (2021).

28. X. Wang, X. Wang, J. Huang, S. Li, A. Meng, Z. Li, Nat. Commun. 12 (2021) 4112.

29. Q. Han, Z. Han, Y. Wang, S. Zhang, J. Fang, H. Li, P. Fang, J. Colloid Interface Sci. 630 (2023) 460–472

30. J. Guo, S. Liang, Y. Shi, C. Hao, X. Wang, T. Ma, PCCP 17 (2015) 28985–28992.

31. M. Sajjad, M. Amin, M.S. Javed, M. Imran, W. Hu, Z. Mao, W. Lu, J. Storage Mater. 43 (2021).

32. W. Ou, J. Pan, Y. Liu, S. Li, H. Li, W. Zhao, J. Wang, C. Song, Y. Zheng, C. Li, J. Energy Chem. 43 (2020) 188–194.

33. U. Gupta, C. Rao, Nano Energy 41 (2017) 49–65.

34. A. Kumar, P. Raizada, A. Hosseini-Bandegharaei, V.K. Thakur, V.-H. Nguyen, P. Singh, J. Mater. Chem. A 9 (2021) 111–153.

35. A. Eftekhari, Appl. Mater. Today 8 (2017) 1–17.

36. C. Xu, S. Peng, C. Tan, H. Ang, H. Tan, H. Zhang, Q. Yan, J. Mater. Chem. A 2 (2014) 5597–5601.

37. V.H. Nguyen, T.P. Nguyen, T.H. Le, D.V.N. Vo, D.L. Nguyen, Q.T. Trinh, I.T. Kim, Q.V. Le, J. Chem. Technol. Biotechnol. 95 (2020) 2597–2607.

38. M. Chhowalla, H.S. Shin, G. Eda, L.-J. Li, K.P. Loh, H. Zhang, Nat. Chem. 5 (2013) 263–275.

39. R.R. Nair, P. Blake, A.N. Grigorenko, et al., Fine structure constant defines visual transparency of graphene, Science 320 (5881) (2008), 1308-1308.

40. S. Larentis, B. Fallahazad, E. Tutuc, Field-effect transistors and intrinsic mobility in ultra-thin MoSe2 layers, Appl. Phys. Lett. 101 (22) (2012), 223104.

41. Z. Zeng, Z. Yin, X. Huang, et al., Single-layer semiconducting nanosheets: high-yield preparation and device fabrication, Angew. Chem. Int. Ed. 50 (47) (2011) 11093–11097.

42. T. Chen, G. Hao, G. Wang, et al., Controlled growth of atomically thin MoSe2 films and nanoribbons by chemical vapor deposition, 2D Mater. 6 (2) (2019), 025002.

43. Y. Li, F. Wang, D. Tang, et al., Controlled synthesis of highly crystalline CVD-derived monolayer MoSe2 and shape evolution mechanism, Mater. Lett. 216 (2018) 261–264.

44. X.L. Luo, Z.Y. Chen, S.Y. Yang, et al., Two-step hydrothermal synthesis of peanut-shaped molybdenum diselenide/bismuth vanadate (MoSe2/BiVO4) with enhanced visible-light photocatalytic activity for the degradation of glyphosate, J. Colloid Interface Sci. 532 (2018) 456–463.

45. I. Siddiqui, H. Mittal, V.K. Kohli, et al., Hydrothermally synthesized micron sized, broom-shaped MoSe2 nanostructures for superior photocatalytic water purification, Mater. Res. Express 5 (12) (2018), 125020.

46. A. Ohtake, Y. Sakuma, Heteroepitaxy of MoSe2 on Si (111) substrates: role of surface passivation, Appl. Phys. Lett. 114 (5) (2019), 053106.

47. Direct observation of the transition from indirect to direct bandgap in atomically thin epitaxial MoSe2, Nat. Nanotechnol. 9 (2) (2013) 111–115.

CHAPTER 4

INSTRUMENTS AND APPARATUS

Major synthesis-related equipment and accessories are addressed in this chapter, along with the operation and working theory of several characterization techniques.

4.1 Crystal Structure Analyses

4.1.1 X-RAY Diffractometer

German physicist Wilhelm Roentgen discovered X-rays in 1895, giving them their name because of their then-unknown nature. These rays, which were invisible and moved instraight lines, had the same effects as regular light on the photographic plate. These rays exhibit greater penetrating strength than light as well. The precise nature of X-rays and the diffraction phenomena of X-rays by crystal atomic planes were adequately discovered in 1912. This finding illuminated the fact that X-rays are waves and opened up a fresh line of inquiry into the composition of matter. As follows are the categories of solid matter:

- **Amorphous:** Similar to the disarray we see in a liquid, the atoms are grouped in an arbitrary manner. Glass is an amorphous material.

- **Crystalline:** The atoms are grouped in a predictable manner, and the crystal is described by repetition of the lowest volume element in three dimensions. A unit cell is the name given to this smallest volume element. Three axes, a, b, and c, as well as the angles between them, alpha (α), beta (β), and gamma (ϒ), represent the dimensions of the unit cell. Crystalline solids make up around 95% of all solids. X-rays are electromagnetic radiation of almost same nature as light but having shorter wavelength of 0.5 to 2.5 Å regions. In the full spectrum, X-rays are located between gamma and ultraviolet photons.

X-rays are electromagnetic radiation of almost same nature as light but having shorter wavelength of 0.5 to 2.5 Å regions. X-rays occupy the region between gamma and ultraviolet rays in the entire spectrum.

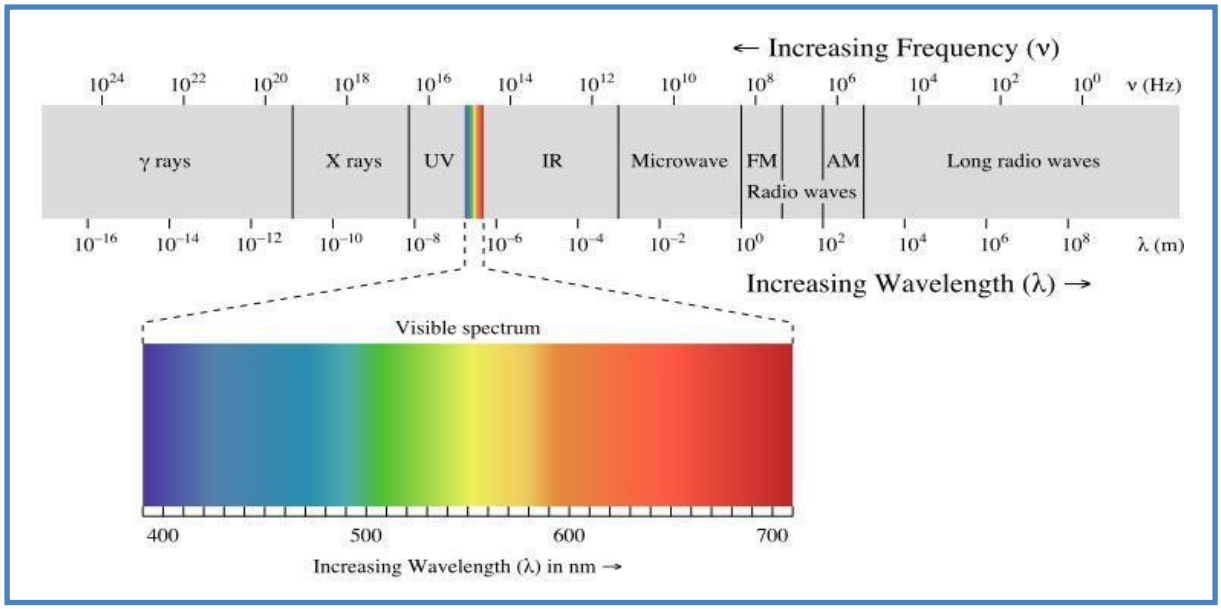

Fig. 4.1: Illustration of electromagnetic spectrum

Diffraction is a scattering phenomenon in which a large number of atoms participate and act as scattering center. X-rays scattered by the atoms which are periodically arranged in the lattice, have definite phase relationship in between them. In some scattering direction, destructive interference takes place but, in few directions, constructive interference occurs andforms the diffracted beam. ***"A diffracted beam may be defined as a beam composed of a large number of scattered rays mutually reinforcing one another."***

- **Working Principle**

In XRD, a collimeter beam of X-rays is incident on a specimen and is diffracted by the crystalline phases in the specimen. Using Bragg equation for first order diffraction, lattice spacing may be found from the diffraction angles. ***Bragg's law*** is the basic law which governs the X-ray diffraction technique of structural analysis. In ***Bragg's law***, the interaction between X-rays and the electrons of the atoms is described as a process of reflection of X-rays by the atomic planes. When monochromatic X-rays incident on the atoms in the crystal lattice, atomic planes allow a part of X-rays to pass through and reflect the other part, there exist a path difference in between the reflected rays from plane 1 and plane 2. These rays willreinforce each other, only when this route difference equates to a wavelength integral multiple.

The ***Bragg's law*** can be written as: $\mathbf{2d\sin\theta = n\lambda}$

Where **n** is an integer and **λ** is the wavelength of the X-rays used, **θ** is Bragg angle and **d** isthe interplanar spacing.

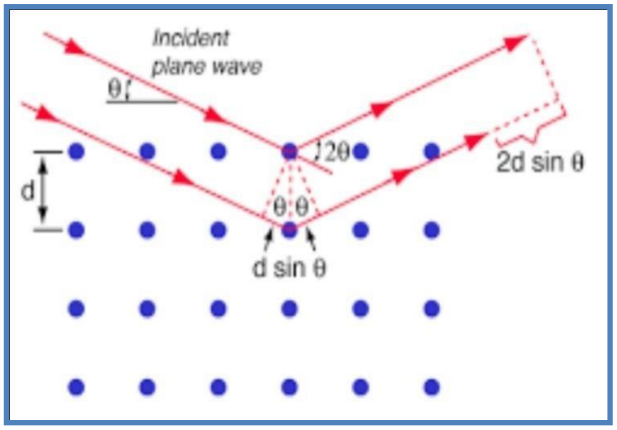

Fig. 4.2: Illustration of Bragg's law

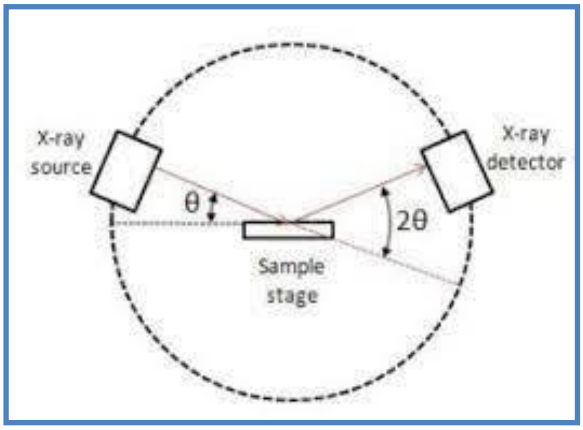

Fig. 4.3: Schematic of X-ray Diffractometer

- **Applications:**

a) Measurement of interplanar spacing between two atomic planes.

b) Determination of orientation of single crystal.

c) Determination of crystal structure for an unknown material.

d) Measurement of particle size, phase and internal stress etc.

A RigakuUltima III X-ray Diffractometer was used for recording the diffraction pattern of the samples in θ-2θ configuration with Cu Kα radiation (λ=1.5404 Å) operated at 40KV voltage and 30mA current. A photographic image of X-ray diffractometer is shown in **Fig 4.4**

Fig. 4.4: Experimental set up of X-Ray Diffractometer

4.2 Optical Property Analysis

4.2.1 Ultraviolet Visible Spectrophotometer

UV spectroscopy is a form of absorption spectroscopy in which molecules absorb light in the ultraviolet range (200–400 nm). The excitation of electrons from the ground state to higher energy states occurs as a consequence of the absorption of UV radiations. Since the ground state and higher energy states have different energies, the energy of the UV light that is absorbed is equal to that difference (E = h).

There are two laws that govern the absorption of light by a medium, known as ***Lambert's law*** and ***Beer's law***. Lambert's law predicts the absorbance is directly proportional to the thickness/path length of the medium. Beer's law explains the effect of concentration ofcolored components in solution on light transmission or absorption. By combining of these two laws, we get ***Lambert-Beer's law*** which is as follows:

$$log\ (I_0/I_t) = A = \alpha cd$$

Where, ***A*** denotes absorbance, ***α*** denotes molar absorptivity, ***c*** is concentration and ***d*** is path length. According to ***Lambert-Beer's law***, the amount of light absorption increases with the number of molecules that can absorb light of a particular wavelength. That is the fundamental idea behind UV spectroscopy.

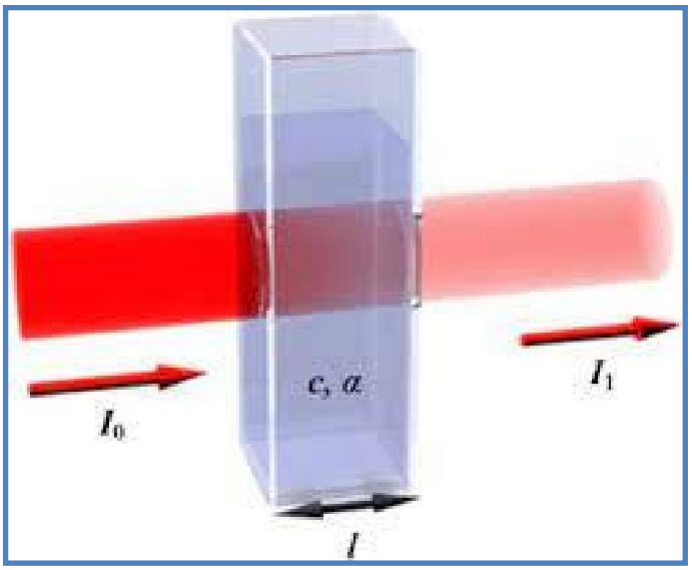

Fig. 4.5: Lambert-Beer's law

- **Configuration of instrument**

An equipment called a spectrophotometer evaluates a sample's transmittance or absorbance in relation to the wavelength of electromagnetic light.The main components of a spectrophotometer are:

1. Source
2. Monochromator
3. Sample container
4. Detectors

1. Source

The ideal light source would have minimal noise, long-term stability, and a consistent intensity across all wavelengths. However, there isn't a source like that, sadly. UV-visible spectrophotometers often employ two sources. A continuous UV spectrum is produced when deuterium or hydrogen is electrically excited at low pressure. A molecular species that is energized and breaks apart into two atomic species and an ultraviolet photon is thought to be the mechanism for this. This is demonstrable by;

$$D_2 + electrical\ energy \rightarrow D_2^* \rightarrow D' + D'' + h\nu$$

Deuterium lamps emit radiation in the range 160-375 nm. These lamps must have quartz cuvettes and windows since glass absorbs light with wavelengths less than 350 nm. Most often, visible light is produced by tungsten filament lamps. In the 350–2500 nm wavelength region, this kind of light is used.

2. Monochromator

All Monochromator contain certain components like ***entrance slit, collimating mirrors, dispersing device (usually a prism or a grating), focusing mirrors and exit slit.*** Radiation of many wavelengths, or polychromatic radiation, enters the monochromator via the entry slit. Following collimation, the beam is directed at an angle towards the dispersion component. The prism or grating divides the beam's wavelengths into their individual components. Only radiation of a certain wavelength exits the monochromator via the exit slit when the dispersing element or the exit slit are moved.

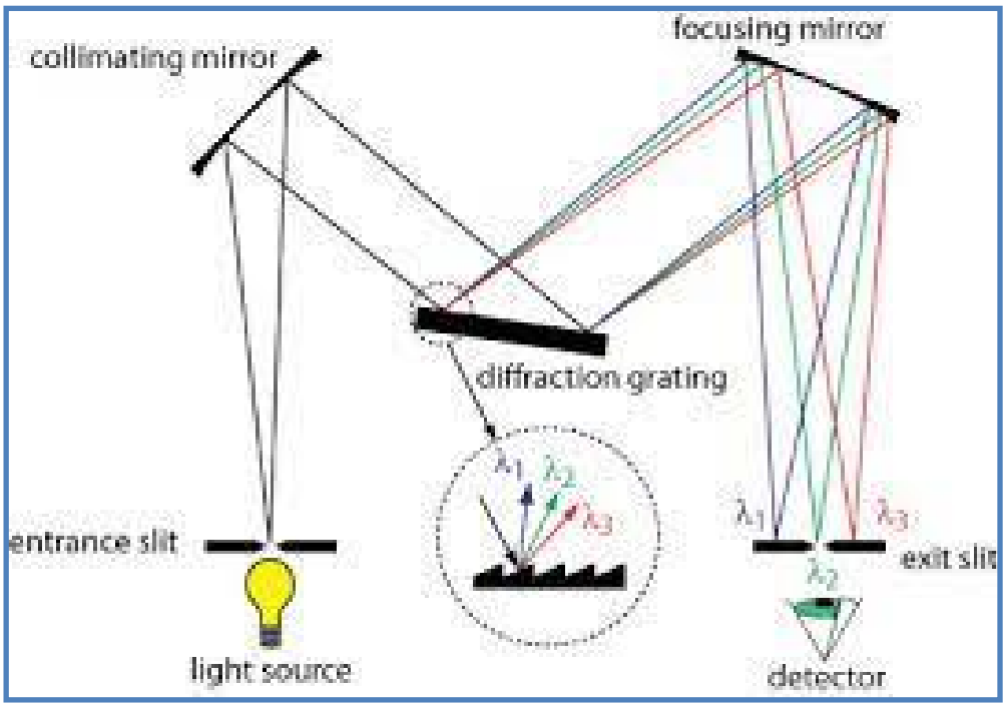

Fig. 4.6: Construction of Monochromator

3. Sample container

The cuvettes (containers) used to hold the reference solution and sample must be transparent to the radiation that will flow through them. For UV spectroscopy, quartz or fused silica cuvettes are necessary. Additionally transparent in the visual range are these cells.

4. Detector

An electrical signal is created from a light signal by a detector. Commonly employed in UV-Vis spectroscopy as a detector is the photomultiplier tube. A photo emissive cathode, numerous dynodes, and an anode make up the device. A photo emissive cathode produces electrons when photons of radiation strike it. A multichannel photon detector is a linear photodiode array, which is another form of detector. These detectors can concurrently measure every component of a scattered radiation beam. Photodiode arrays are intricate gadgets with exceptional durability due to their solid-state construction.

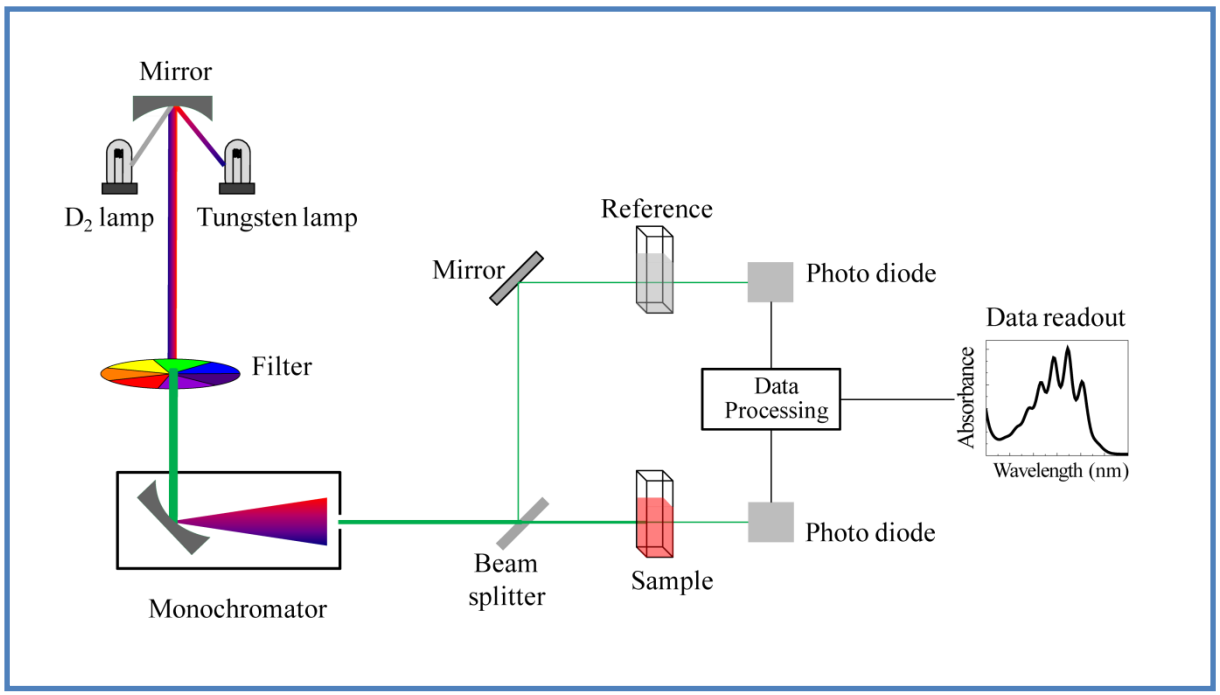

Fig. 4.7: Configuration of Uv-Visible spectrophotometer

Fig. 4.8: Experimental set up of UV-VIS-NIS (SHIMADZU UV-3600) Spectrophotometer

4.2.2 Raman Analysis

Dr. C.V. Raman made the first observation of Raman scattering in 1928 and utilized it to examine the vibrational states of several substances.

- **Raman system**

A typical Raman system consists of the following basic components:

1) Excitation source, usually a laser
2) Optics for sample illumination
3) Double or triple Monochromator
4) Signal processing system

A sample is fixed to the sample chamber, and a lens directs laser light towards it. Another lens is employed to gather the dispersed light, which is then focussed at the Monochromator's entry slit. The monochromator disperses incoming radiation while efficiently rejecting stray light. A detector's surface is illuminated by the light that emerges from the monochromator's exit slits after being gathered and concentrated. Within the detector, the optical signal is transformed into an electrical signal that is then further processed by detector electronics. For each set frequency interval, a signal of this kind is saved in computer memory. Scanning the Monochromator is used to assess the light intensity at different frequencies in a standard Raman system employing a photomultiplier tube (PMT) detector. Its Raman spectrum is shown by a plot of signal strength vs wavenumber.

- **Principle**

In a process known as Rayleigh scattering, a sample is exposed to a powerful monochromatic light source (often a laser), the most of which is scattered by the sample at the same wavelength as the incoming laser radiation. A little percentage of the incoming light, around one photon in a million, gets scattered, but at a wavelength that is different from the laser's original wavelength. The sample is excited by laser light, which scatters in all directions. A portion of this dispersed light was directed towards the Raman spectrum detector, which captures it. This spectrum displays the light at the original laser (Rayleigh) frequency as well as the sample-specific Raman spectral characteristics.

The same transitions between molecular vibrational states (M) and (M*) in the infrared absorption can also result in Raman scattering. A key difference between the Raman and infrared processes is that, in the former process, the photons involved are not absorbed or emitted but rather shifted in frequency by an amount corresponding to the energy of the particular vibrational transition. In the Stokes process, which is the parallel of absorption, the scattered photons are shifted to lower frequencies as the molecules abstract energy from the exciting photons; in the anti-Stokes process, which is parallel to emission, the scattered photons are shifted to higher frequencies as they pick up the energy released by the molecules in the course of transitions to the ground state.

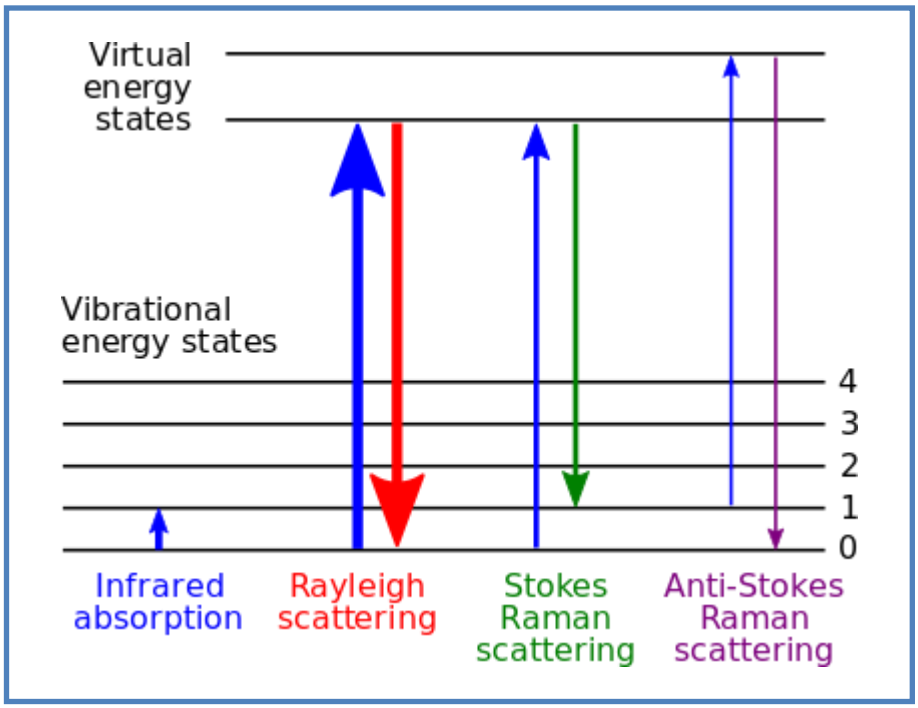

Fig. 4.9: Different types of scattering

Relaxation from the virtual state occurs almost instantaneously and is predominantly to the initial ground state. This process results in Rayleigh scatter, which is scattered light of the same wavelength as the excitation laser. Relaxation to the first excited vibrational levelresults in a Stokes-Raman shift. Stokes-Raman shift scattered light is of lower energy (longer wavelength) than that of the laser light. In addition, most systems have at least a small population of molecules that are initially in an excited vibrational state. When the Raman process initiates from the excited vibrational level, relaxation to the ground state is possible, producing scatter of higher energy (shorter wavelength) than that of the laser light. This type

of scatter is called anti-Stokes Raman scatter. Two molecules can give exactly the same Raman spectrum, and the intensity of the scattered light is proportional to the amount of material present. Thus Raman provides both qualitative and quantitative information about the sample. The Raman spectra carried out by WITEC alpha 300R-RAMAN spectroscopy.

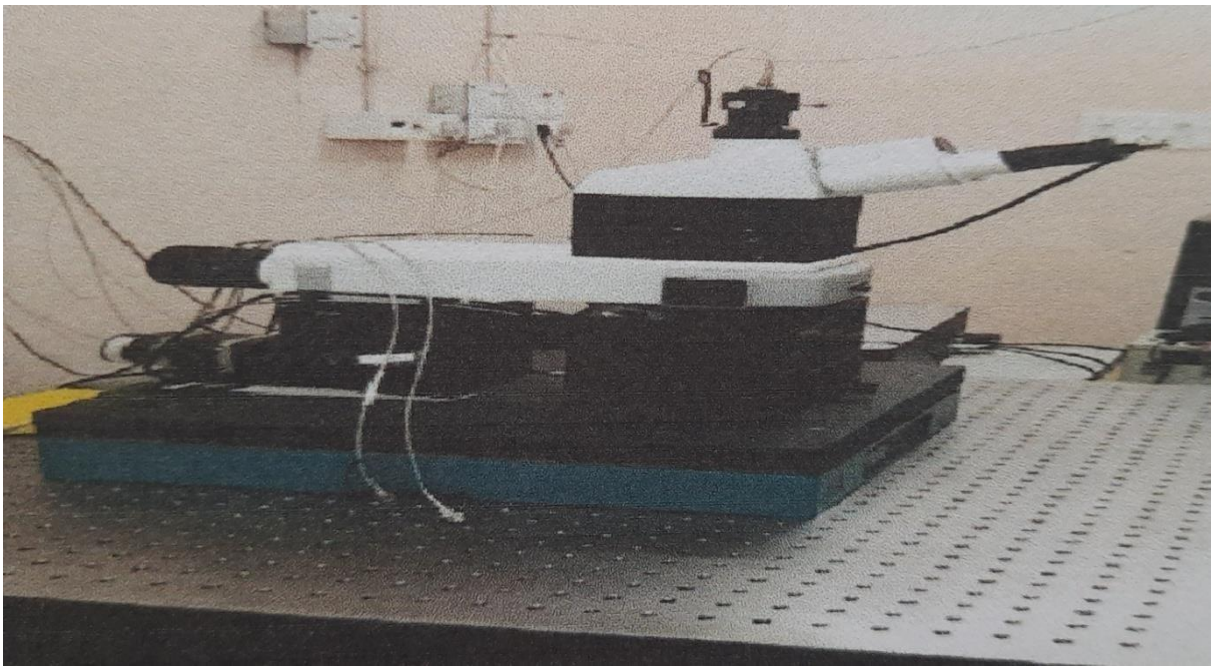

Fig. 4.10: Raman Analysis (WITEC) Setup

4.3 Morphological analysis

4.3.1 Field Emission Scanning Electron Microscope (FESEM)

The Greek words micros (little) and skopeo (look at) are the origin of the term microscope. Since the advent of science, there has been a desire to examine the world around us in ever-increasing depth. Our human eye provides the extreme limitation in microscopy.It has a resolution ρeye of ~0.1 mm which is equivalent to the diameter of a human hair. This means that two small objects placed about 20 cm from the eye can be viewed as distinct whenthey are ~0.1 mm apart. The limitation arises from the intrinsic magnification power of human eye and the separation of the sensing elements on the retina. And optical microscope has a resolution Gama ρopt and improvement of ρopt than that of the unaided eye can be done in a way which is limited by the wavelength of the light used to illuminate the object. For visible light, this corresponds to ρopt ~0.2 μm. That's why below 0.2 μm , we cannot visualize objects through optical microscope. A FESEM is an electron microscope whichuses electron beam liberated by field emission source instead of light.

Electrons will not travel far through air and electron microscopes are usually vacuum based instruments. Image formation in the SEM depends on the signals produced from the electron beam and specimen interactions. These interactions can be classified into two major categories: ***elastic interactions and inelastic interactions***. The incoming electron's deflection by the specimen's atomic nucleus or outer shell electrons causes elastic scattering. Very little energy is lost during the collision, and the dispersed electron changes direction at a large angle, defining this kind of interaction. Backscattered electrons (BSE), incident electrons that are elastically dispersed at an angle greater than 90 degrees, give a signal that is helpful for imaging the material. The main beam electron of inelastic scattering transfers a significant amount of energy to the sample atom via various interactions between the incoming electrons and the electrons and atoms of the sample. Whether the specimen electrons are stimulated singularly or collectively, as well as the binding energy of the electron to the atom, determine how much energy is lost. The secondary electron emission signal is the one that is most often employed as a result of the main electron beam's interaction with the sample. Secondary electrons are loosely bound electrons that may be released when the main beam reaches the sample surface, ionizing the specimen atoms. As theyhave low energy, typically an average of around 3-5 eV, they can only escape from a region within a few nanometers of the material surface. These can be used to give information about the surface topography, morphology of the sample with good resolution. In addition to these signals, a number of other signals are produced when an electron beam strikes a sample, including the emission of ***continuous X-rays, characteristic X-rays, Auger electrons and cathodoluminescence***.

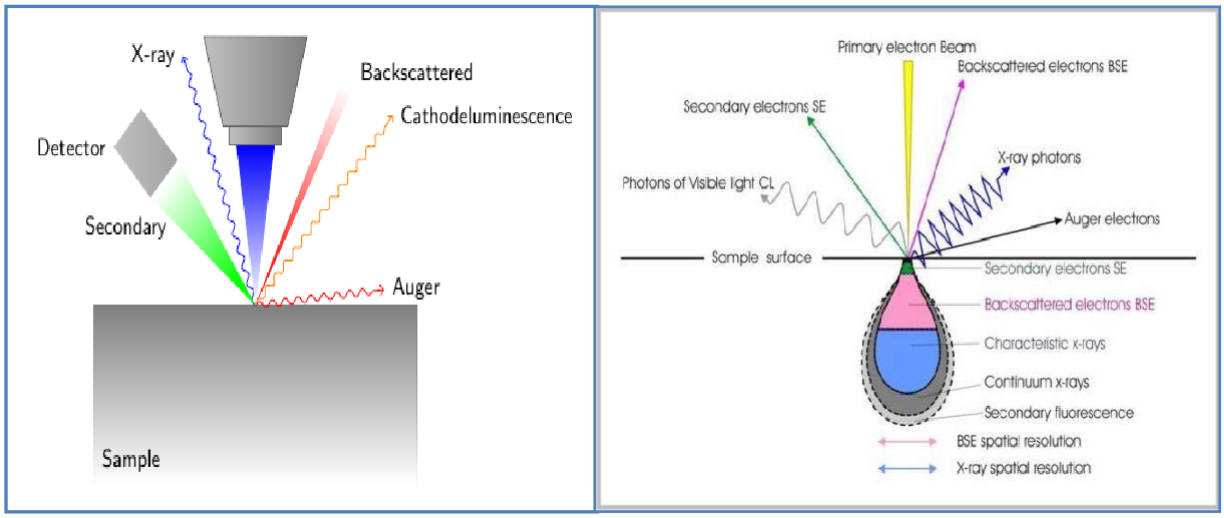

Fig. 4.11: Interaction of electron beam with matter

- **Configuration of FESEM**

The complete breakdown of the field emission scanning electron microscope is shown in detail in **Fig. 4.11.** The electron gun, electromagnetic lenses, and aperture used to concentrate the electron beam, a detector, a vacuum system, and an electron gun make up this apparatus.

- **Electron Gun**

A steady electron beam with a high current, a narrow spot, variable energy, and minimal energy dispersion is produced by the electron cannon. The majority of first-generation SEM systems employed thermionic emission sources, such as tungsten "hairpin" (= 4.5eV) or lanthanum hexaboride (LaB6) (= 2.4eV) cathodes. However, the tendency for recent SEMs is to use field emission sources, which provide increased current and reduced energy dispersion. Another crucial consideration in choosing electron sources is emitter lifetime. The most popular electron cannon is made up of three components, as illustrated in **Fig. 4.12**: a Wehnelt cylinder, an anode, and a V-shaped hairpin tungsten filament (the cathode).

The work function of the metal has to be overcome by thermoionic sources at a high temperature in order for the electrons to escape from the cathode. Although they are affordable and need little upkeep, they have certain drawbacks that limit their use, such a limited lifespan, poor brightness, and a wide energy spread. Field emission guns (FEG) are an excellent substitute for thermionic electron guns for contemporary electron microscopes. The electron source in the FEG is a single crystal tungsten wire with a highly sharp tip. In this device, a powerful electric field develops on the tip's fine orientation, drawing electrons in the direction of the anodes to create a focused electron stream.

- **Electron Lenses**

Electrostatic or magnetic fields may concentrate an electron beam. However, the magnetic field-controlled electron beam has less aberration, therefore the SEM system simply uses the magnetic field. To create a magnetic field, wire coils known as "electromagnets" are utilised, and the current provided to these coils allows for precise control over the electrons' paths.

- **Condenser lens**

After leaving the emission source and going through the anode plate, the electron beam will diverge. The electron beam is converged and collimated into a comparatively parallel stream using the condenser lens. A copper coil that generates a magnetic field is often placed between two pieces of iron that are rotationally symmetric. The electron beam may pass through a hole in the core of the pole pieces. The magnetic field concentrates the electron beam to the lens-gap that separates the two pole components. By altering the condenser lens current, the focus point's location may be changed.

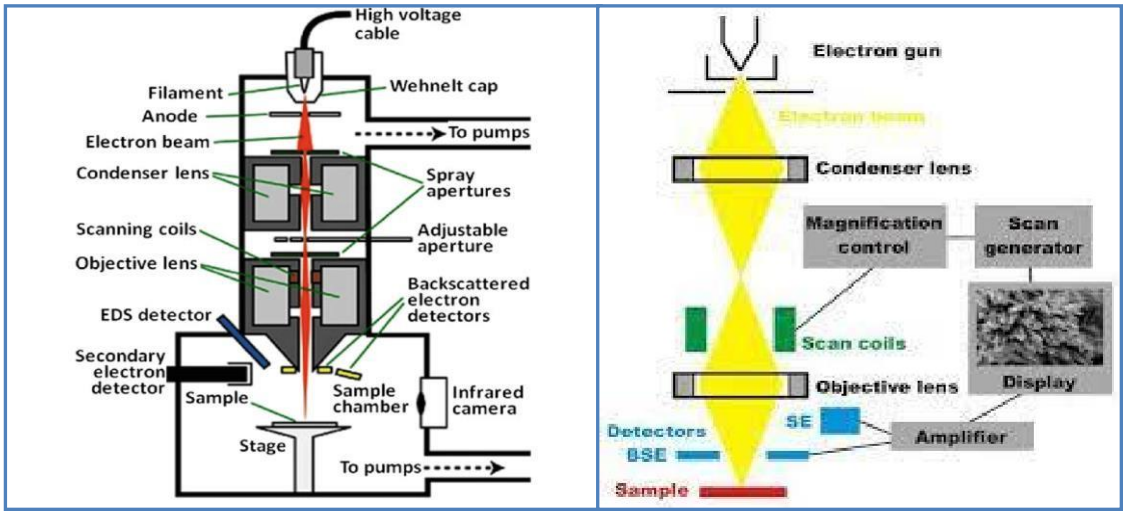

Fig. 4.12: Configuration of FESEM and its different components

- **Scan coils**

The electron beam is deflected across the item in a zigzag pattern by the scan coils. Synchronously with this scan movement, the picture on the display begins to take shape. The scan velocity controls how often the screen refreshes and how much noise is present in the picture. Lower and upper coils are often used in scan coils to avoid the creation of a circular shadow at low magnification.

- **Objective lens**

The objective or "probeforming" lens is situated directly above the material at the bottom of the electron column. After passing through the apertures below the condenser lens, the beam diverges once again and has to converge. The sample's ultimate size and location are controlled by the objective lens, which concentrates the electron beam on it.

- **Sample preparation**

Since the FESEM is a vacuum-based device, as we just explained, the sample must be vacuum-tolerant. Additionally, a sample might be harmed or destroyed by intense electron radiation due to heating or other factors. Samples may be coated with gold or platinum under the microscope to preserve the real surface features, even in pretty excellent vacuum (10-8mbar). Insulating samples may get charged under an electron beam and deflect the incoming electron beam. This reduces the resolution and often necessitates some kind of preventative approach, such covering the sample with a conductive layer.

Fig. 4.13: FESEM (Hitachi S-4800) set up

4.3.2 Transmission Electron Microscope (TEM):

In the microscopy method known as transmission electron microscopy (TEM), an electron beam is passed through a material to produce an image. The specimen is often a suspension on a grid or an ultrathin slice that is no thicker than 100 nm. The interactions of the electrons with the specimen as the beam travels through it result in an image. The picture is then magnified and focused using an imaging device, such as a fluorescent screen, a sheet of photographic film, or a sensor like a scintillator connected to a charge-coupled device.

Diffraction, spectroscopy, scanning TEM imaging (STEM), conventional imaging, and combinations of these are among the operating modes of TEM equipment. Even with conventional imaging, there are

several fundamentally different ways that contrast is created, or "image contrast processes." Atomic number (abbreviated as "Z contrast" using the standard abbreviation for atomic number Z), crystal structure or orientation (abbreviated as "crystallographic contrast" or "diffraction contrast"), position-to-position variations in thickness or density (referred to as "mass-thickness contrast"), the slight quantum-mechanical phase shifts that individual atoms cause in electrons that pass through them (referred to as "phase contrast"), or other factors can all cause contrast. Each contrast mechanism gives the operator a different sort of information depending on the contrast mechanism and how the microscope is used—the settings of the lenses, apertures, and detectors. This implies that a TEM is capable of providing a tremendous range of data at the nanometer and atomic scales, and in ideal cases shows not only the positions of all atoms but also the kind of atoms they are and the kinds of relationships they make with one another. As a result, TEM is acknowledged as an essential tool for nanoscience in the fields of biology and materials.

- **Components of HRTEM:**

An electron emission source for generating the electron stream, an electron vacuum system in which the electrons travel, a number of electromagnetic lenses, and electrostatic plates are some of the components that make up HRTEM. The latter two allow the user to manipulate and direct the beam anyway they see appropriate. The ability to insert, move, and remove specimens from the beam path requires a mechanism as well. Imaging devices are then used to create a picture utilising the electrons that exit the system.

- **Vacuum System**

  In order to increase the mean free path of the electron gas interaction, traditional HRTEM is evacuated to low pressures, generally on the order of 10-4 Pa. This is required in order to prevent an arc from forming when there is a voltage difference between the cathode and the ground, as well as to significantly reduce the frequency of electron collisions with gas atoms, also known as the mean free path. The system must be able to re-evacuate since HRTEM components like film cartridges and specimen containers must be frequently inserted or replaced. As a consequence, HRTEMs are equipped with a number of pumping systems and airlocks and are not entirely vacuum sealed. The vacuum system that is utilised to evacuate a HRTEM to a functioning pressure level goes through many steps. After attaining a low or roughing vacuum using either a rotary vane pump or a diaphragm pump, which establishes a low enough pressure to permit its function, a turbo-molecular or diffusion pump is utilised to achieve the high vacuum level necessary for operations. In order to enable the low vacuum pump to operate intermittently while the turbo-molecular pumps operate constantly, the vacuum side of a low-pressure pump may be linked to chambers that house the exhaust gases from the turbomolecular pump. distinct vacuum levels may

be isolated in distinct HRTEM components using pressure-limiting apertures, such as a higher vacuum of 10-4 to 10-7 Pa or higher in the electron gun in high-resolution or field-emission HRTEMs.

- **Specimen Stage:**

HRTEM specimen stage designs include airlocks to let the specimen holder enter the vacuum with the least amount of vacuum loss in other areas of the microscope.

The specimen holders may handle sample grids that are a standard size as well as self-supporting specimens. The thickness and mesh sizes of the conventional HRTEM grid, which has a thickness of 3.05 mm, range from a few to 100 m. The sample is received in a meshed area with a diameter of about 2.5 mm. The usual grid materials include platinum, gold, molybdenum, and copper. This grid is sent to the sample holder, which is attached to the specimen stage. A variety of stage and holder designs are available, depending on the kind of experiment being conducted. 2.3 mm grids are also sometimes, albeit sparingly, employed in addition to 3.05 mm grids. In the mineral sciences, where specimen material might be highly rare and a large amount of tilt may be required, these grids were mostly used. The precise value varies on the accelerating voltage, although specimens that are electron transparent often have a thickness of less than 100 nm.

After being positioned within a HRTEM, the sample must be moved in order to put the area of interest to the beam, as in single grain diffraction, in a certain orientation. To meet this, the HRTEM stage offers sample movement in the XY plane, Z height adjustment, and typically simply one tilt orientation perpendicular to the axis of side entry holds. Sample rotation may be accomplished on dedicated diffraction holders and stages.

Double-tilt sample holders, which are specialist holder designs that provide two orthogonal tilt angles of movement, are present in several modern HRTEMs. Some stage designs, such as top-entry or vertical insertion stages that were historically popular for high resolution TEM research, may only have X-Y translation available. The design parameters for HRTEM stages are complex due to the combined needs of mechanical and electron-optical constraints, and there are unique models available for different procedures.

- ## Electron Gun:

The basic components of an electron cannon are the filament, a biassing circuit, a Wehnelt cap, and an extraction anode. By connecting the filament to the negative component power supply, electrons may be "pumped" from the electron cannon to the anode plate and the HRTEM column, completing the

circuit. The objective of the gun is to create an electron beam that leaves the assembly at a predetermined angle, also known as the gun divergence semi-angle, or. By making the Wehnelt cylinder have a larger negative charge than the filament itself, divergent electrons that leave the filament are, when operated properly, pushed into a converging pattern, the minimum size of which is the gun crossover diameter.

- **Electron lens:**

In order to simulate the behaviour of an optical lens, electron lenses concentrate parallel electrons at a predetermined focal distance. Magnetic or electrostatic principles may be used to operate electron lenses. The majority of HRTEM electron lenses use electromagnetic coils to create a convex lens. For the lens's field to remain radially symmetrical, the magnetic lens' radial symmetry must be preserved; otherwise, astigmatism and other aberrations like spherical and chromatic aberration would increase. Electron lenses are made of iron, iron-cobalt, or nickel-cobalt alloys like permalloy. Based on their magnetic properties, such as permeability, hysteresis, and magnetic saturation, they are selected.

The parts include the yoke, the magnetic coil, the poles, the polepiece, and the external control electronics. The symmetry of the pole piece affects the boundary conditions for the magnetic field that generates the lens. Construction errors in the pole piece may lead to serious distortions in the magnetic field's symmetry, which will eventually impair the lenses' ability to reconstruct the object plane. The exact size of the gap, the internal diameter and taper of the pole piece, as well as the overall design of the lens, are typically determined by a finite element analysis of the magnetic field while taking into consideration the design's thermal and electrical restrictions.

- **Apertures:**

Apertures are annular metallic panels that allow electrons that are too far from the optic axis to pass through to be excluded. These are made of a thin metallic disc that allows axial electrons to flow through but prevents other electrons from doing so. Apertures reduce beam intensity as electrons are filtered out of the beam, which may be desired in the case of beam-sensitive samples. This permission of centre electrons in a HRTEM causes two effects concurrently. Second, this filtering eliminates electrons that are scattered at high angles for a variety of reasons, including chromatic or spherical aberration or diffraction from internal sample interactions. Condenser lenses, for example, have fixed apertures within the column. Other apertures, however, can be adjusted in the plane perpendicular to the beam path or inserted or removed from the beam path. Aperture assemblies are mechanical tools that enable the user to choose between various aperture sizes and trade off the intensity and filtering effect of the aperture. Micrometres are frequently included in aperture assemblies in order to change

the aperture when optical calibration is necessary.

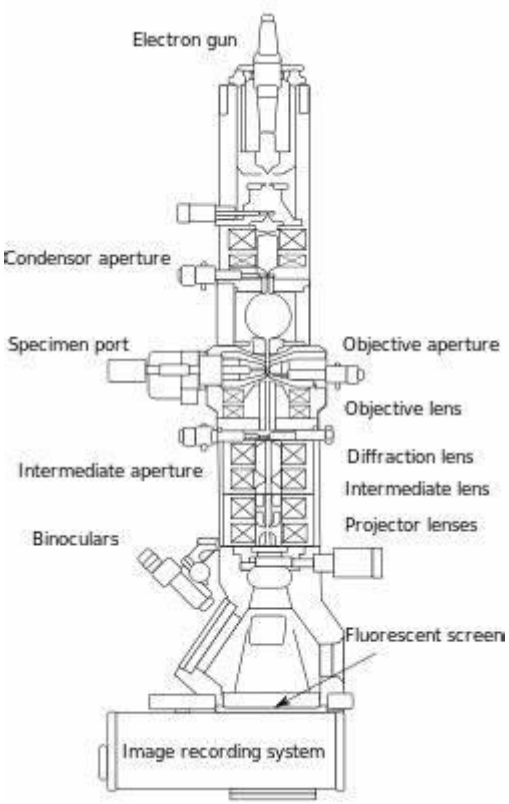

Fig:4.14 Schematic Diagram of HRTEM

- **Image Contrast and Interpretation:**

  The contrast in a high-resolution transmission electron microscopy picture is caused by interference between the electron wave and itself in the image plane. We cannot preserve the phase of an electron wave, just the amplitude in the picture plane. However, a significant percentage of the sample's structural information is recorded in the phase of the electron wave. It has to be found by adjusting the aberrations of the microscope (such defocus) to convert the wave's phase at the specimen exit plane into amplitudes in the picture plane. A qualitative grasp of the connection between the electron wave and the sample's crystal structure may be swiftly gained despite the relationship being complex. Each imaging electron has a unique interaction with the material. In general, the electron wave above the sample may be compared to a plane wave that has incident on the sample surface. As it enters the sample, it is drawn in by the positive atomic potentials of the atom cores and channels down the atom columns of the crystalline lattice (sstate model). The

interaction of the electron waves in distinct atom columns results in Bragg diffraction concurrently. The perfect description of dynamical electron scattering in a material that does not meet the weak phase object approximation—which is almost all actual samples—remains the pinnacle of electron microscopy.

However, enough is known about the physics of electron scattering and the production of electron microscope pictures to enable precise modelling of such images.

Fig. 4.15 FEI Tecnai TEM

4.4 Surface Analysis

4.4.1 X-Ray Photoelectron Spectroscopy

X-Ray Photoelectron Spectroscopy is one of the most powerful surface analytical techniques capable to provide accurate qualitative elemental analysis (for all elements except hydrogen and helium), quantitative composition and determination of chemical state such as binding and oxidation can also be done. The information should be originated within ~10 nm from theouter surface.

- **Principles of XPS**

XPS is based on the photoelectric effect which is discovered by Hertz in 1887. In this case, electron emission from the surface is resulted due to the interaction of an x-ray photon of sufficient energy with the solid surface. The applied x-ray of 1-15 KeV energy is capable to induce electrons not only from the outer shells but also from the core levels of all elements of periodic table. The governing equation of this phenomenon is as follows:

$$h\nu = E_b + E_{kin} + W_f$$

Where, E_b is binding energy, E_{kin} is kinetic energy of photoelectron, W_f is work function of the instrument.

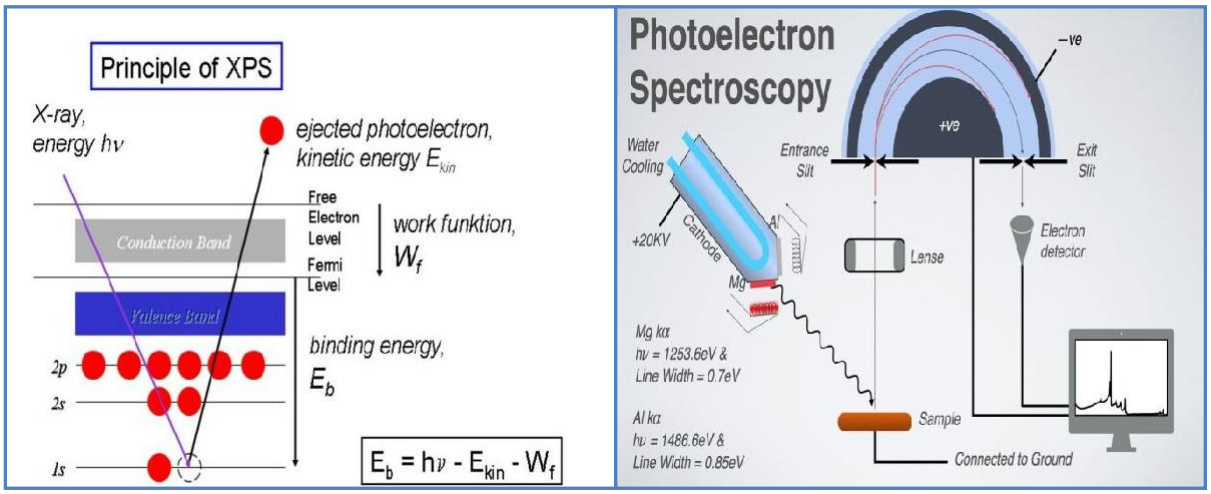

Fig. 4.16: Basic principles and constructions of XPS

- **Configuration of XPS instrument**

The primary components of the experimental setup are (i) an X-ray source for XPS, (ii) an electron energy analyzer with a detection system, and (iii) a sample stage, all of which are housed within a vacuum chamber. As with most approaches, a computer, often equipped with software that enables mathematical treatment as illustrated in Fig. 4.14, operates and controls the system.

- **X-ray source**

Since XPS is concerned with the analysis of core electrons from a solid surface, sources used in XPS must be able to produce photons of a sufficient energy to access a suitable number of core electron levels. Photons of this energy lie within the X-ray region of the electromagnetic spectrum. As a result, these are otherwise referred to as X-rays. X-ray tube produce X-rays by directing a sufficiently energetic electron beam at some metallic solid. This metallic object is referred to as the X-ray anode, with the electron source being the cathode. Although any solid can in principle be used as an X-ray anode, Al has become that most commonly used in XPS due to the relatively high energy and intensity of Al-Kα X-rays, the minimal energy spread of Al-Kα X-rays and the fact that Al is an effective heat conductor.

- **Electron energy analyzer**

Since information in XPS is derived from the E_{kin} of the electron emissions, effective analysis requires energy filter that exhibits both a high-energy resolution and a high transmission. The former allows for the separation of closely spaced peaks, thereby optimizing speciation identification capabilities, while the latter allows for sensitivity to be maximized. The two primary energy filter configuration used in XPS named ***Cylindrical Mirror Analyzer (CMA), Concentric Hemispherical Analyzer (CHA).***

- **Detector**

In XPS, it is not only important to measure the energy of the electron emissions but also the number of electrons produced. XPS spectra is plotted in units of energy versus intensity, with the energy defined by the energy analyzer used and the intensity defined by the number of electrons recorded by the detector. To obtain the best possible sensitivity, the detector must be capable of recording individual electrons, that is, operating in pulse counting mode. This signal is recorded in units of current (A), which are then represented in units of counts per second.

- **Sample stage**

It is important to put the samples on the sample holder in a manner that ensures electrical conductivity. Bolt-down assemblies or metallic clips may be used to accomplish this. An alternative is a tape that has metal loaded on it. Powders may be formed into indium foil or carbon tape by applying pressure to the individual particles.

- **Vacuum requirement**

As XPS is a surface sensitive method, impurities can play a major role in the observed spectra. The criterion is that a good vacuum is needed to maintain the integrity of the surface. In general, 10^{-5}Torr is sufficient to allow the Photoelectron to reach the detector without suffering collisions with other gas molecules. On the other hand, 10^{-9}Torr or lower is requiredto keep an active surface clean for more than several minutes. So, 10^{-8} - 10^{-9}Torr provides a reasonable pressure range for XPS measurement. Sample analysis was performed on the SPECS with hemispherical energy analyzer (HAS 3500). Photoelectrons were excited using the monochromatic Mg Kα X-ray (1253.6eV) or Al Kα X-ray (1486.6eV) was used as the excitation source operated at 10 kV and with an anode current 17 mA.

The photograph of the X-ray Photoelectron Spectroscopy is shown in the **Fig.4.15.**

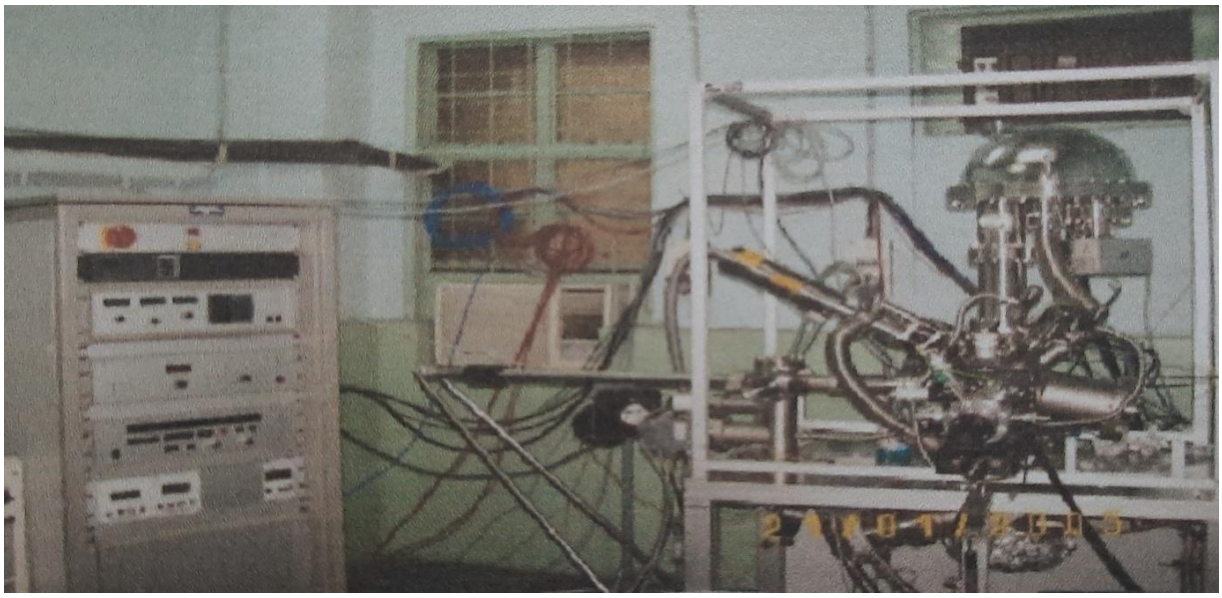

Fig. 4.17: Experimental set up of XPS

4.5 Electrochemical property analysis

4.5.1 Cyclic Voltammetry

The most used method for gathering qualitative data regarding electrochemical processes is cyclic voltammetry. It provides quick localization of the electroactive species' redox potentials.

Fig.4.18: Cyclic Voltammetry (GAMRY-auto lab) setup

When the voltage hits V2, the scan is reversed and the voltage is swept back to V1, unlike in cyclic voltammetry when the voltage is swept between two values at a predetermined rate. Below is an example of a typical voltammogram for a single electrode transfer reaction. Once again, there is just one electrochemical reactant in the solution. The CV record has a few well defined criteria for an electrochemical process that is reversible.

1. The voltage separation between the current peak is cyclic.
2. The positions of peak voltage do not alter as a function of voltage scan rate.
3. The ratio of the peak currents is equal to one.
4. The peak currents are proportional to the square root of the scan rate.

- **Principle**

The use of a voltage is essential for triggering an electrode response because it affects electron transfer and energy levels. A volt is only the energy needed to transport charge, as can be shown by looking at the units of volts V= Joule/Coulomb. Electrical energy is therefore produced by applying a voltage to an electrode. An applied voltage may change the "energy" of the electrons within a metal electrode since electrons have a charge. By taking into account the Fermi level, it is possible to somewhat comprehend how electrons behave in a metal. Atoms in metals are densely packed and strongly overlapped with one another. As a result, a chunk of metal lacks the distinct individual electron energy levels that one would find in an atom of the same substance. In place of a continuous level structure, states are formed with the available electrons filling them from the bottom up. The energy where the top "electrons" reside is known as the Fermi level.

Fig. 4.19: Autolab PGSTAT (M204) potentiostat/galvanostat Setup

Chapter 5
Synthesis and HER kinetic of MoSSe

5.1 Experimental Section:

5.1.1 Synthesis of MoSSe:

- **Materials:**

Sodium Molybdate Dihydrate ($Na_2MoO_4.2H_2O$) from Alfa Aesar, Selenium powder (Se powder) from Merck, Thiourea ($H_2N{-}C(=S){-}NH_2$) from Mark were used for synthesis. Deionized (DI) water was taken from a Direct-Q Millipore deionized (18 Ω at 25°C). [1]

- **Sample Preparation:**

1. MoSSe was prepared by Hydrothermal method. To start the process at first 60mg of $Na_2MoO_4.2H_2O$ was taken in a 500ml biker with 30ml of DI water then Sonicate it for 10min.
2. Then another 500ml biker with 40ml DI was taken and 20mg of Se powder weighted and mixed. Then the it also sonicated for 30min.
3. Now another biker with 20ml DI was taken and 20mg ($H_2N{-}C(=S){-}NH_2$) was added and left for sonication for 20min.
4. Now both the solution was mixed in a biker and poured into a autoclave for 24hr in 200℃.

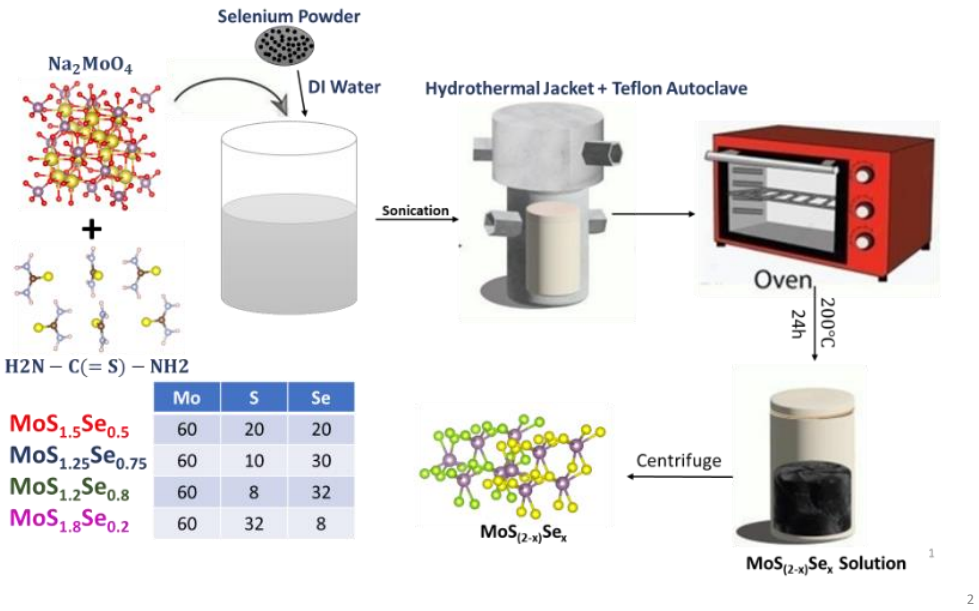

	Mo	S	Se
$MoS_{1.5}Se_{0.5}$	60	20	20
$MoS_{1.25}Se_{0.75}$	60	10	30
$MoS_{1.2}Se_{0.8}$	60	8	32
$MoS_{1.8}Se_{0.2}$	60	32	8

Fig.1 Schematic diagram of MoSSe synthesis using hydrothermal process.

5.1.2 Characterizations

- The phase purity and crystal structure of the different layers of as synthesized MoSSe nanosheet material was characterized by X-Ray diffraction (XRD, D8 Advance ECO, Cu-Kα radiation, (λ=1.54Å)).
- The chemical structures of different layers of MoSSe nanosheet were analyzed by Raman spectroscopy by confocal Raman spectrometer (alpha 300, Witec, Germany, Laser Source of wave-length 532 nm).
- The surface analysis of MoSSe was done by using X-ray photoelectron Spectroscopy.
- The morphology analysis of the prepared samples was done by High Resolution Transmission Electron Microscopy (HRTEM, JEOL-200kV).
- The Field Emission Scanning Electron Microscopy (FESEM) picture provides a comprehensive depiction of the fundamental morphological characteristics shown by nanoparticles or nanosheets within the size range of 500 nm to 5 µm.

5.2 Structural Study:

The diffraction patterns of the synthesised powder samples were collected using a Rigaku MiniFlex powder X-ray diffractometer. The measurements were conducted throughout a scattering angle range of $15° \leq 2\theta \leq 80°$, with a step size of 0.02°. Monochromatic Cu Kα radiation was used, and the measuring speed was set at 0.5° min^{-1}. The d-value observed at a distance of 0.53 nm corresponds to the lattice plane with Miller indices (100) in the crystal structure of MoO_3[2-4]. This finding suggests the possible production of MoSSe−MoO_3(JCPDS No.29-0914).The X-ray diffraction (XRD) pattern of the MoSSe sample exhibits three distinct peaks at angles of 34.3°, 42.7°, and 56.4°.

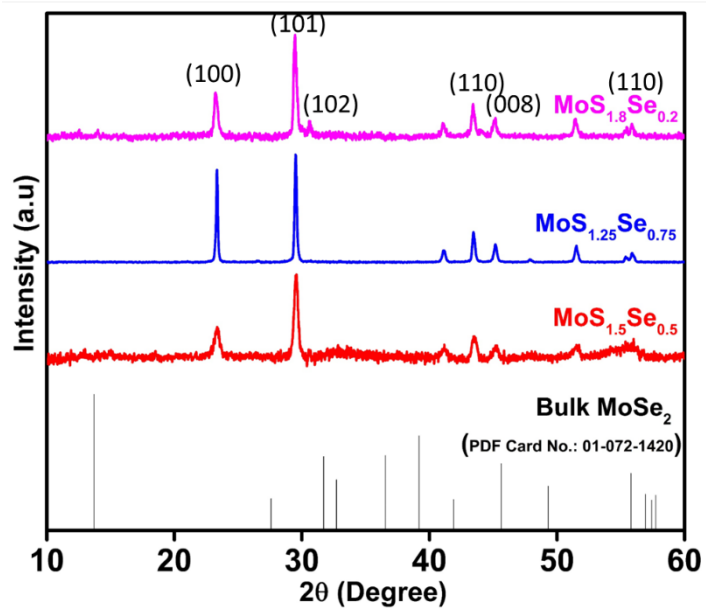

Fig. 2 shows the XRD pattern of the prepared sample.

5.3 Morphological Analysis:

5.3.1 Field Emission Scanning Electron Microscopy (FESEM):

Fig.3 shows the morphology of the synthesised materials, as seen using field emission scanning electron microscopy (FESEM). The progressive change in the morphology of the samples is attributed to the observed variation in the concentration of S and Se source. It is evident that all of the samples exhibit nanoflower-like morphologies [3,5], as seen **Fig.3 (a-d)**. In addition, the use of an energy dispersive spectrometer (EDS) was employed to identify the presence of the elements Mo (shown in violet), Se (also indicated in violet), and S (indicated in green) in **Fig. 3(e),** therefore verifying their uniform distribution.

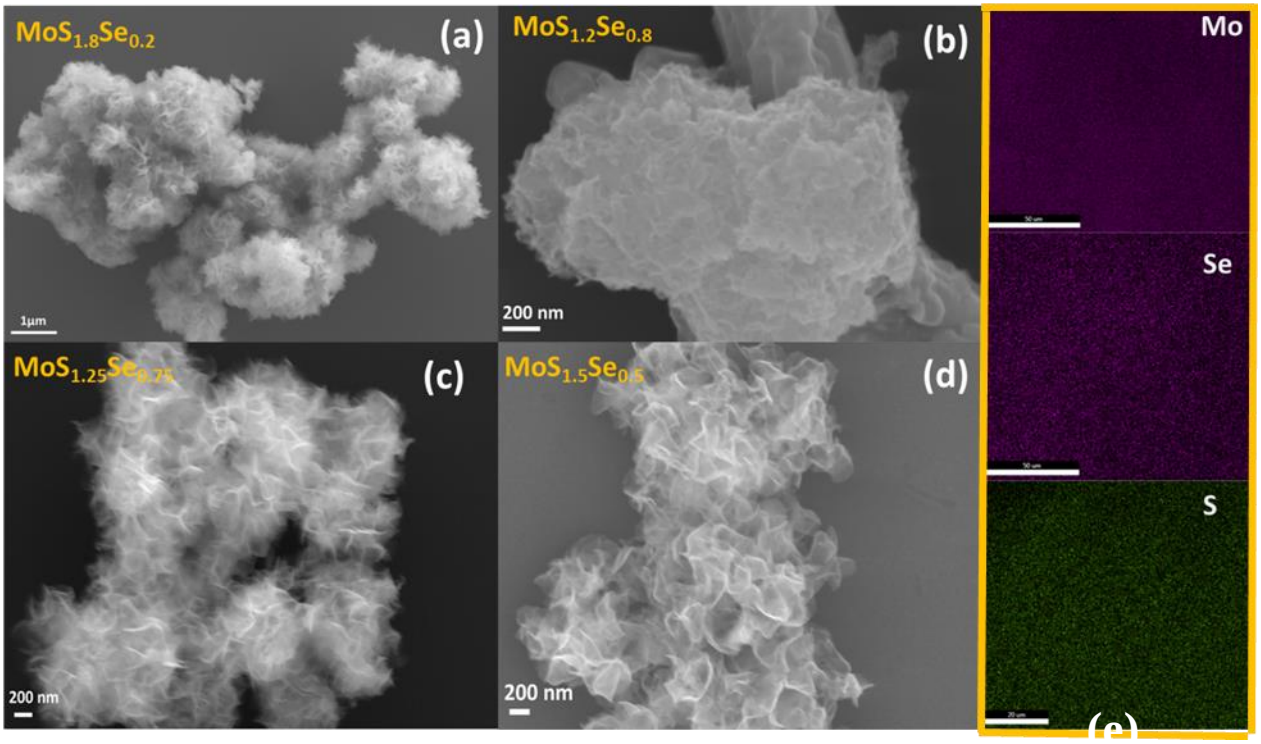

Fig.3 FESEM image of (a) $MoS_{1.8}Se_{0.2}$ (b) $MoS_{1.2}Se_{0.8}$ (c) $MoS_{1.25}Se_{0.75}$ (d) $MoS_{1.5}Se_{0.5}$ (e) The elemental mapping images of Mo, S and Se element for $MoS_{1.8}Se_{0.2}$

5.3.2 Transmission Electron Microscope (TEM):

The precise structure of the as-prepared MoSSe is further elucidated by the high resolution transmission electron microscopy (TEM) images shown in Figure 4(a), 4(b), 4(c) and 4(d). Figure 5(a) illustrates the flower-like morphology of MoSSe and the presence of curved fringes in the as-prepared MoSSe sample [6,7,8]. The measured d-spacing, which refers to the distance between the lattice fringes, is around 0.688 nm (**Fig.5(b)**). This value closely corresponds to the separation seen between the (002) planes of hexagonal MoSSe [9]. Fig displays the selected area electron diffraction (SAED) pattern of the nanomaterial in its original state, providing evidence of its polycrystalline structure.

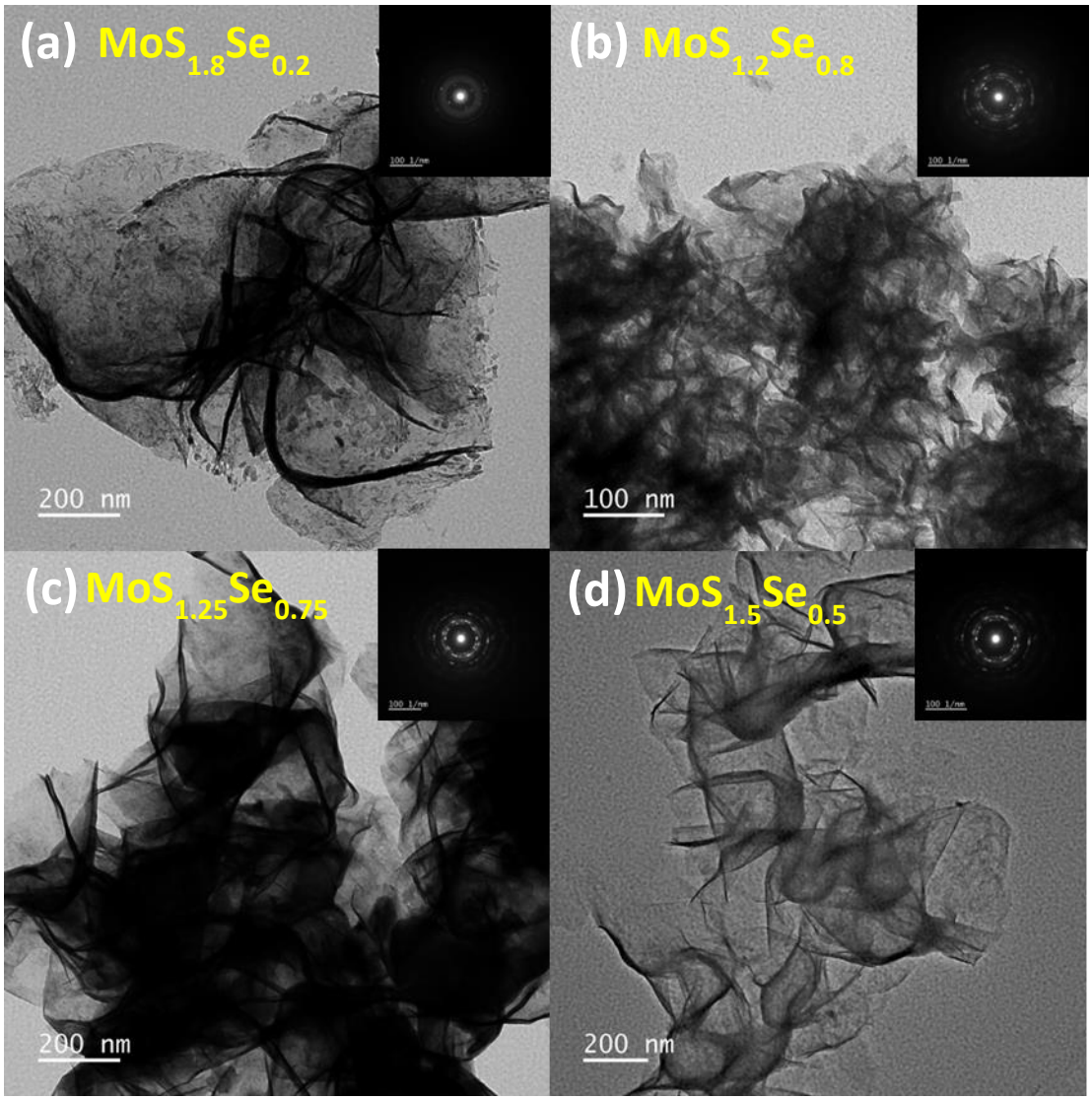

Fig. 4 TEM image of (a) $MoS_{1.8}Se_{0.2}$ (b) $MoS_{1.2}Se_{0.8}$ (c) $MoS_{1.25}Se_{0.75}$ (d) $MoS_{1.5}Se_{0.5}$ with SAED pattern

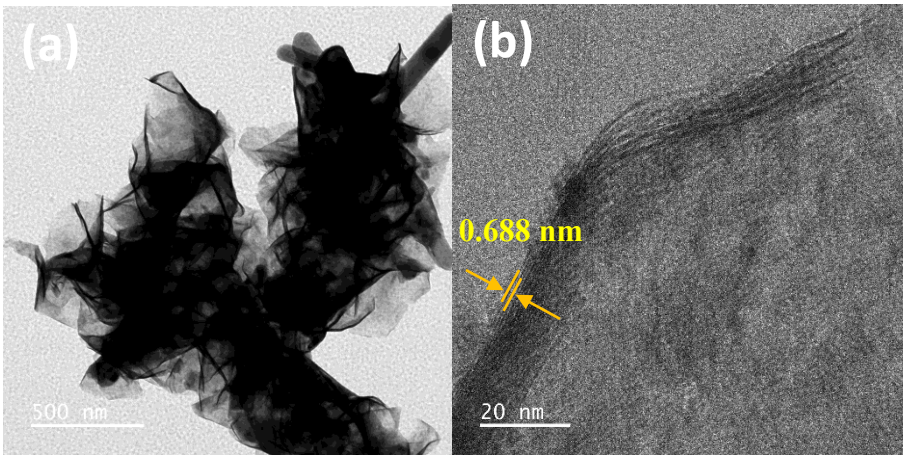

Fig. 5 (a)TEM image of (a) $MoS_{1.8}Se_{0.2}$ (b) high resolution TEM images for $MoS_{1.8}Se_{0.2}$ particles

5.4 Surface Analysis:

X-ray photoelectron spectroscopy (XPS) analysis was conducted in order to assess the elemental compositions and chemical states of the $MoS_{1.8}Se_{0.2}$ samples. The X-ray photoelectron spectroscopy (XPS) study reveals the presence of Mo, S, Se and O components in the hybrid material. The high resolution Mo3d (figure 6(a)) and Se3d(figure 6(b)) shows that the peak is located at 233.16,228.9 eV correspond to the $Mo^{4+}3d_{3/2}$ and $Mo^{4+}3d_{5/2}$ component of MoSSe respectively two other peak 229.79 and 233.82 eV in the high resolution Mo3d spectrum was assigned to $Mo3d_{5/2}$ and $Mo3d_{3/2}$ of Mo^{6+} and the peak at 530.78 eV in the O1s spectrum (Fig. 6(d)) could be ascribed to the lattice oxygen in MoO_3[10-13].

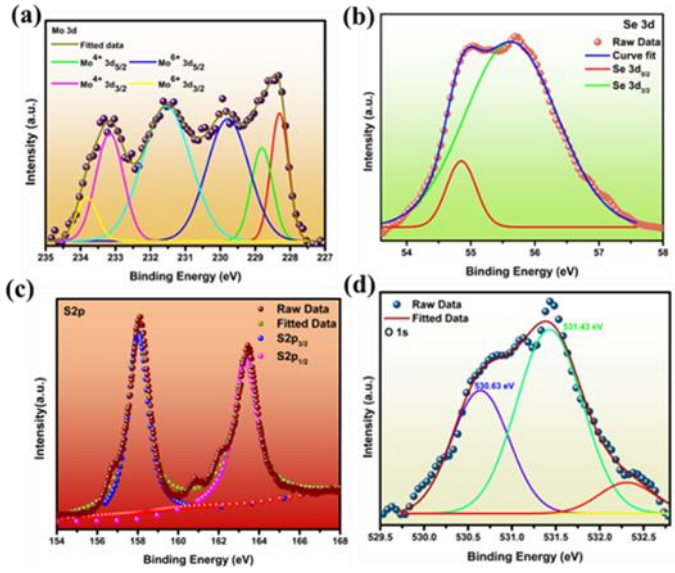

Fig.6 High resolution scans of (a) Mo3d, (b) Se3d (c) S and (d) O1s electrons.

5.5 Experimental HER activity:

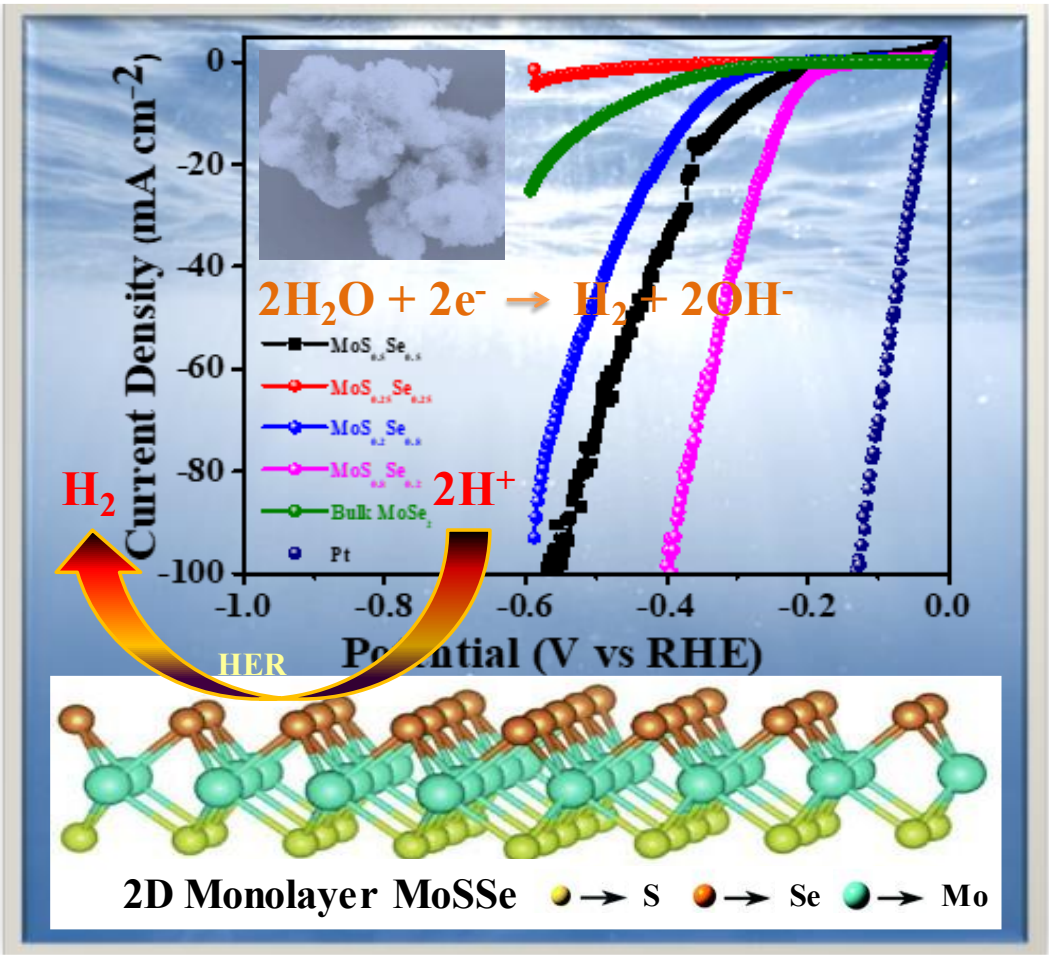

Fig.7 Schematic diagram of HER of MoSSe

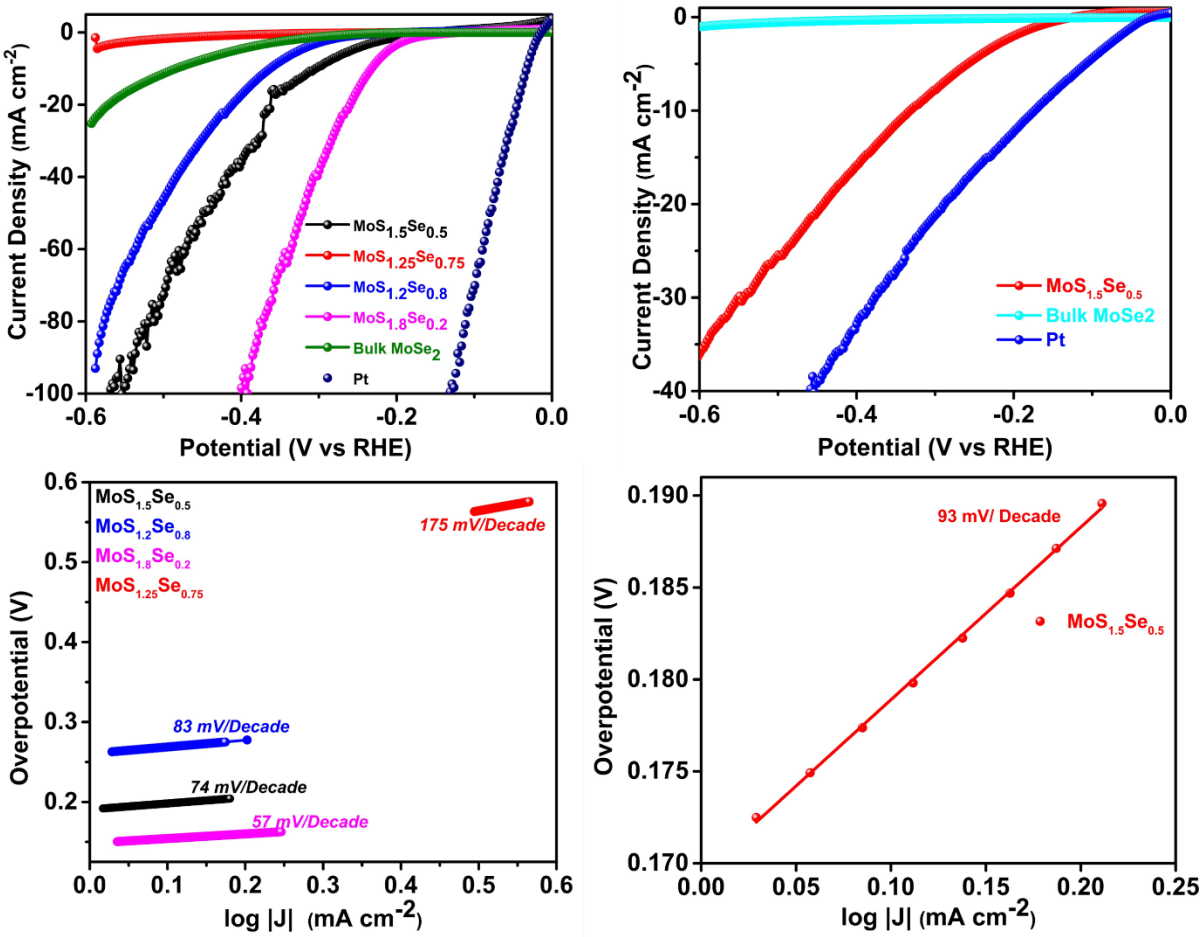

Fig.8: Electrocatalytic HER performance of MoSSe composite. (a,c) Polarization curves and (b,d) Tafel slope in 0.5 M H_2SO_4 and 1 M KOH solution of MoSSe composite.

The promising acidic and basic hydrogen evolution reaction of MoSSe composite has been shown in figure 5. It has been observed that the overpotential for HER kinetics changes with varying concentrations of sulphur (S) and selenium (Se). Generally, lower overpotential at 10 mA cm^{-2} is essential to measure for acidic HER kinetics. Among the MoSSe composites, $MoS_{1.8}Se_{0.2}$ shows lower overpotential (η~210 mV/decade) in comparison to $MoS_{1.5}Se_{0.5}$ (η~225 mV/decade), $MoS_{1.2}Se_{0.8}$ (η~350 mV/decade) and $MoS_{1.25}Se_{0.75}$ (η~450 mV/decade) respectively. Moreover, $MoS_{1.8}Se_{0.2}$ exhibits lower Tafel slope of 57 mV dec^{-1} than $MoS_{1.5}Se_{0.5}$ (74 mV/decade), $MoS_{1.2}Se_{0.8}$ (83 mV/decade) and $MoS_{1.25}Se_{0.75}$ (175 mV/decade). The lower Tafel slope of $MoS_{1.8}Se_{0.2}$ composite indicates favorable binding of hydrogen on the active sites and follows Volmer–Tafel HER

mechanism. Therefore, enhancement of HER kinetics is strongly dependent on stoichiometry of sulphur and selenide. At lower se concentrations, the adsorption of hydrogen becomes facile whereas at high concentrations, the reaction becomes sluggish. The phenomenon is mainly attributed as, at low concentrations of Se, defect density is lower and uneven charge distribution at S and Se interface facilitates the hydrogen adsorption. Whereas at higher concentration of Se, defect density is high where strong adsorption of hydrogen deaccelerates the HER kinetics [14,15].

Similarly, $MoS_{1.5}Se_{0.5}$ shows alkaline HER performance at overpotential 320 mV at 10 mA cm^{-2} current density and Tafel slope of 93 mV/decade.

To estimate the electrochemical double layer capacitance (C_{dl}) of MoSSe composite, cyclic voltammetry (CV) is measured at non Faradic region of -0.15 V vs. RHE to 0.15 V vs. RHE (Figure 6). $MoS_{1.2}Se_{0.8}$ shows C_{dl} of 3.2 mF cm^{-2}, which is higher than $MoS_{1.5}Se_{0.5}$ (0.135 mF cm^{-2}) and $MoS_{1.8}Se_{0.2}$ (3.2 mF cm^{-2}) respectively.

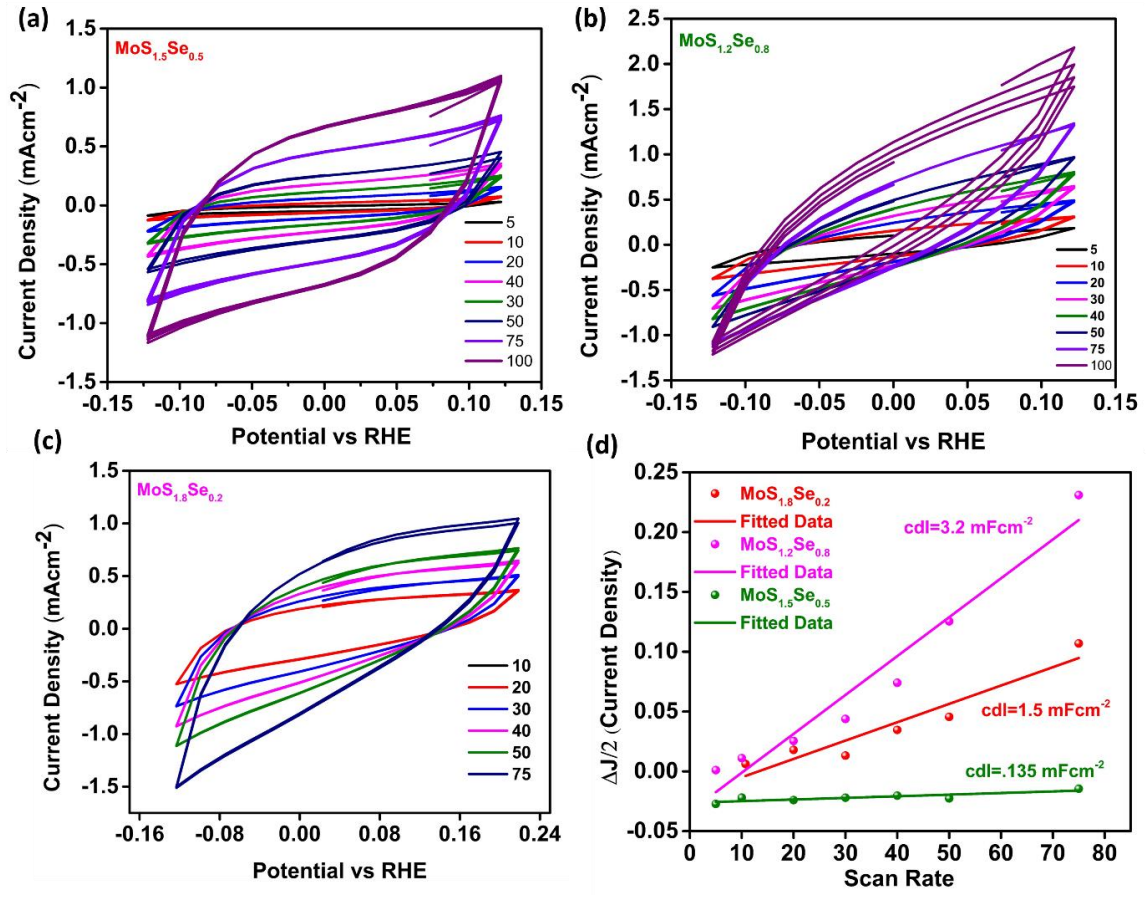

Fig.9; Cyclic Voltammetry (CV) of (a) $MoS_{1.5}Se_{0.5}$ (b) $MoS_{1.2}Se_{0.8}$ and (c) $MoS_{1.8}Se_{0.2}$ at non-Faradic region. (d) Comparison of double layer capacitance.

As a demonstration, this work emphasizes the importance of sulphur selenium interface on MoSSe composite for the catalytic role of highly active pH-insensitive electrocatalysts. Furthermore, theoretical predict will need to be considered in future for charge transfer mechanism at the interface and catalytic role on pH universal HER catalysis.

5.6 Conclusion:

This study presents findings indicating that the introduction of S into molybdenum Di selenide ($MoSe_2$) results in enhanced electrochemical reactivity in comparison to unadulterated $MoSe_2$. The produced S-Se unsaturation in $MoS_{1.8}Se_{.2}$ shows outstanding HER and $MoS_{1.8}Se_{0.2}$ exhibits lower Tafel slope of 57 mV dec^{-1} . This study introduces a viable methodology for altering the electrical configuration of electrocatalysts to enhance the efficacy of hydrogen generation. Additionally, it offers opportunities to gain expertise in the development of highly efficient electrocatalysts derived from Earth-abundant materials, with potential uses in forthcoming energy systems.

Reference:

1. Singh, S.; Deb, J.; Sarkar, U.; Sharma, S. MoS2/MoO3 nanocomposite for selective NH3 detection in a humid environment. ACS Sustainable Chem. Eng. 2021, 9, 7328−7340.
2. Duraisamy, S.; Ganguly, A.; Sharma, P. K.; Benson, J.; Davis, J.; Papakonstantinou, P. One-Step Hydrothermal Synthesis of Phase Engineered MoS2/MoO3 Electrocatalysts for Hydrogen Evolution Reaction. ACS Appl. Nano Mater. 2021, 4, 2642−2656
3. T. J. S. Anand and S. Shariza, Electrochim. Acta, 2012, 81, 64.
4. R. Harpeness, A. Gedanken, A. M. Weiss and M. A. Slifkin, J. Mater. Chem., 2003, 13, 2603
5. S. X. Yang, H. Y. Yang, H. Y. Ma, S. Guo, F. Cao, J. Gong and Y. L. Deng, Chem. Commun., 2011, 47, 2619.
6. S. X. Yang, H. Y. Yang, H. Y. Ma, S. Guo, F. Cao, J. Gong and Y. L. Deng, Chem. Commun., 2011, 47, 2619.
7. S. X. Yang, H. Y. Yang, H. Y. Ma, S. Guo, F. Cao, J. Gong and Y. L. Deng, Chem. Commun., 2011, 47, 2619.
8. K. Tang, Y. Qian, J. H. Zeng and X. G. Yang, Adv. Mater., 2003, 15, 448.
9. Q. H. Wang, K. K. Zadeh, A. Kls, J. N. Coleman and M. S. Strano, Nat. Nanotechnol., 2012, 7, 699
10. D. Duphil, S. Bastide, J. C. Rouchaud, J. L. Pastol, B. Legendre and C. L. Cle´men, Nanotechnology, 2004, 15, 828
11. Y. D. Ma, Y. Dai, C. W. Niu, L. Yu and B. B. Huang, J. Phys. Chem. C., 2011, 115, 202371
12. S. Larents, B. Fallahazad and E. Tutuc, Appl. Phys. Lett., 2012, 101, 223104
13. S. Y. Hu, Y. C. Lee, J. L. Shen, K. W. Chen, K. K. Tiong and Y. S. Huang, Solid State Commun., 2006, 139, 176
14. Maiti, A.; Srivastava, S. K. Ru-Doped CuO/MoS2 Nanostructures as Bifunctional WaterSplitting Electrocatalysts in Alkaline Media. ACS Appl. Nano Mater. 2021, 4 (8), 7675–768
15. Li, B.; Ma, J. G.; Cheng, P. Silica-Protection-Assisted Encapsulation of Cu2O Nanocubes into a Metal–Organic Framework (ZIF-8) To Provide a Composite Catalyst. Angew. Chemie - Int. Ed. 2018, 57, 6834–6837.

Chapter 6
Conclusion and Future Scope

6.1 Conclusion:

In conclusion, the synthesis of $MoSe_{2-x}S_x$ has been successfully accomplished by a one-pot hydrothermal method. The introduction of S-Se unsaturation in MoSSe might induce micro strain due to the mismatch in atomic sizes, hence facilitating phase engineering. Moreover, $MoSe_{1.8}S_{0.2}$ exhibits a phase concentration, indicating significant conductivity, substantial interlayer spacing, exceptional hydrophilicity, and a considerable specific surface area. In addition, it has been shown that $MoSe_{1.8}S_{0.2}$ has remarkable efficacy as a catalyst for the hydrogen evolution reaction (HER), while also demonstrating exceptional durability across several cycles. The result offers a framework for successfully creation of S-Se unsaturation.

6.2 Scope of Future Work:

The two-dimensional nanomaterial MoS2 is very captivating due to its novel physical properties and promise for many applications. There are many reasons why we consider this finding to be significant. The development of a straightforward spectroscopic technique for the determination of thickness and lateral dimensions is crucial, as it would greatly facilitate the characterization of liquid-exfoliated nanosheet dispersions. These findings will also enable the production of liquid-suspended nanosheets with precise control over their length and thickness distributions. The investigation of size effects on the basic physical characteristics of layered inorganic materials is crucial. Additionally, understanding the impact of nanosheet size is significant for many applications, such as fluorescence spectroscopy in solution. The aforementioned approaches possess a general nature and may be effectively used to a diverse array of two-dimensional materials, such as WS_2, $MoSe_2$, and WSe_2. This work emphasises the impact of the nanosheet's edge on its collective electrical and optical characteristics.

In order to facilitate the progress of future energy technologies, it is essential to develop electrocatalysts composed of non-noble metals that exhibit exceptional performance and economic benefits for the hydrogen evolution reaction (HER). Materials based on MoS2, specifically two-dimensional transition-metal sulphides, are considered to be very promising catalysts for the hydrogen evolution reaction (HER). Doping engineering has been shown as an effective way for modifying the electrocatalytic activity of these materials. This study presents a practical approach for manipulating the electrical structure of electrocatalysts to enhance their performance in hydrogen generation and oxygen reduction. It also gives insights into the development of highly efficient electrocatalysts using Earth plentiful materials, which hold promise for future energy applications.